

**THE FABRICATION AND CHARACTERIZATION  
OF IRON DISULFIDE [FeS<sub>2</sub>]  
PHOTOELECTROCHEMICAL (PEC) SOLAR CELL**

HIS THESIS HAS BEEN ACCEPTED FOR  
THE DEGREE OF M.Sc 1998  
AND A COPY MAY BE PLACED IN THE  
UNIVERSITY LIBRARY.

**BY**

**WAITA SEBASTIAN M.**

A Thesis Submitted in Partial fulfillment for the award of a Master's degree [Physics] at  
the University of Nairobi.

**UNIVERSITY OF NAIROBI  
LIBRARY  
P. O. Box 30197  
NAIROBI**

1997

UNIVERSITY OF NAIROBI LIBRARY



0133222 0

## DECLARATION

This Thesis is my original work and has not been presented for examination in any other University.

WAITA SEBASTIAN M.

SIGN.....

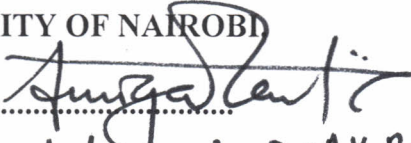
DATE.....13/11/98

This work has been presented for examination with our authority as supervisors.

1. DR. A. K. RATURI,

PHYSICS DEPT,

UNIVERSITY OF NAIROBI

SIGN:.....

DATE:.....23/11/98 for Dr AK Raturi

2. DR. B. O. ADUDA,

PHYSICS DEPT,

UNIVERSITY OF NAIROBI.

SIGN:.....

DATE:.....13/11/98

The Scientist verse

Great are the works of the Lord, studied by all  
Who have pleasure in them

Psalms 111:2

## DEDICATION

To my parents, brothers and sisters.

UNIVERSITY OF NAIROBI  
GHROMO LIBRARY

## ACKNOWLEDGEMENTS

I am greatly indebted in thanks to my supervisors Dr. A. K. Raturi and Dr. B. O. Aduda for their encouragement, guidance and constructive criticism and helpful suggestions which made this work a success. I sincerely thank Prof. R. O. Genga, former head of Physics Dept, University of Nairobi, and Prof. B. O. Kola, current Chairman Physics Dept, University of Nairobi, for their support in some matters pertaining to this work.

I certainly appreciate the assistance given to me by the management of the Departments of Physics and Chemistry, University of Nairobi, in allowing me to use their laboratory facilities. Many thanks go to the technical staff of both Physics and Chemistry Departments, University of Nairobi, for their assistance. Special thanks to Ms Rose Mutungi of Chemistry Dept, University of Nairobi for her special and memorable assistance in the due course of this work. I thank Mr. Waiganjo of Physics Dept, University of Nairobi for his co-operation and willingness to assist while I undertook this work.

Much appreciation to my friends and especially Mr. Kennedy Thiong'o for the outstanding concern and understanding he showed me at a critical time I did this work.

Thanks to my parents, brothers, cousins and all other relatives for the unceasing concern, patience, moral support and understanding for the period of time I was doing this work.

I am grateful to the University of Nairobi for availing a scholarship thus enabling me do this work.

## CONTENTS

	PAGE
ACKNOWLEDGEMENTS.....	(i)
LIST OF TABLES.....	(v)
LIST OF FIGURES.....	(vii)
LIST OF SYMBOLS.....	(x)
ABSTRACT.....	(xiii)
CHAPTER ONE	1
1 INTRODUCTION.....	1
1.1 LITERATURE REVIEW.....	5
1.1.1 The photoelectrochemical solar cell.....	5
1.1.2 Progress in semiconductor-liquid junction solar cells.....	6
1.1.3 Semiconductor electrode materials for photoelectrochemical solar cells.....	8
1.1.4 Drawbacks of photoelectrochemical solar cells.....	9
CHAPTER TWO	13
2 THEORETICAL BACKGROUND.....	13
2.1 Introduction.....	13
2.2 Design of photoelectrochemical solar cells.....	15
2.3 Processes at the semiconductor electrolyte boundary.....	23
2.4 Interface of semiconductor-electrolyte.....	28

2.5 The effect of illumination.....	30
2.6 Photoemission into electrolyte.....	34
2.7 Charge separation by electric field in the semi-conductor.....	36
2.8 Photovoltaic measurements.....	40
2.9 Spectral response.....	42

CHAPTER

CHAPTER THREE	43
---------------	----

3 EXPERIMENTAL PROCEDURE.....	43
-------------------------------	----

3.1 Introduction.....	43
-----------------------	----

3.2 Preparation of samples and solar cell study.....	47
--	----

3.2.1 Optimization of parameters.....	47
---------------------------------------	----

3.2.2 Preparation of iron disulfide.....	48
--	----

3.2.3 Photoelectrode preparation.....	52
---------------------------------------	----

3.2.4 Iron disulfide characterization.....	54
--	----

3.2.5 Photoelectrochemical solar cell studies.....	55
--	----

CHAPTER FOUR	61
--------------	----

4 RESULTS AND DISCUSSION.....	61
-------------------------------	----

4.1 Optimization of parameters.....	61
-------------------------------------	----

4.2 Characterization of iron disulfide film.....	62
--	----

4.3 Photoanode transmittance studies.....	67
---	----

4.4 Electrolyte studies.....	70
------------------------------	----

4.5 Transmittance of cell container.....	72
4.6 Photoelectrochemical solar cell .....	74
4.7 Spectral response of photoelectrochemical solar cell.....	82
4.8 Stability of photoelectrochemical solar cell.....	84

Table 4.1

CHAPTER FIVE	87
5 CONCLUSION AND RECOMMENDATIONS FOR FUTUR WORK.....	87
5.1 Conclusion.....	87
5.2 Recommendations for future work.....	88
REFERENCES.....	90

Table 4

Table 4

Table 4

Table 4.7

Table 4.8

Table 4.9



## LIST OF TABLES

	PAGE
Table. 4.1 Optical transmittance for iron pyrite film.....	65
Table. 4.2 Optical transmittance for a photoanode before use in the cell.....	68
Table. 4.3 Optical transmittance for a photoanode after use in the cell.....	68
Table. 4.4 Optical transmittance (%) of electrolyte in the visible wavelength range.....	71
Table. 4.5 Optical transmittance (%) of cell container in the visible wavelength range..	72
Table. 4.6 Photocurrent and photovoltage values on illumination for photoanode A.....	74
Table. 4.7 Electrical output values for photoanode A for photoelectrochemical solar cell fabricated in our laboratory.....	76
Table. 4.8 Photocurrent and photovoltage values on illumination for photoanode B.....	76
Table. 4.9 Electrical output values of photoanode B obtained from PEC solar cell.....	78

Table. 5.0 Spectral sensitivity of photoelectrochemical solar cell.....82

Table. 5.1 Values of photocurrent density within a period of seven (7) days for PEC solar cell....84

Fig. 2.1 Schem

Fig. 2.2 Bar

Fig. 2.3 Energy

excit

Fig. 2.4 Effi

elect

Fig. 2.5 Ener

on illu

Fig. 2.6 Typ

solar cell

Fig. 3.1 Schem

## LIST OF FIGURES

	PAGE
Fig. 2.1 Schematic diagram of a photoelectrochemical (PEC) solar cell.....	16
Fig. 2.2 Band shapes in the bulk of an illuminated n-type semi-conductor.....	19
Fig. 2.3 Energy relations between semi-conductor and redox couple in solution controlling electron exchange.....	24
Fig. 2.4 Effect of illumination on depletion layer and electron transfer reaction at semi-conductor-electrolyte interface.....	37
Fig. 2.5 Energy relations in depletion layer for conduction band edge Fermi level in dark and on illumination.....	39
Fig. 2.6 Typical current-voltage curve for an ideal solar cell.....	41
Fig. 3.1 Schematic diagram of the spray pyrolysis setup.....	46

UNIVERSITY OF NAIRU  
CHIRAMP LIBRARY

Fig. 3.2 Schematic experimental setup of the sample annealing in sulfur vapour.....	51
Fig. 3.3 PEC solar cell setup.....	58
Fig. 3.4 Spectral response measurements for PEC solar cell.....	60
Fig. 4.0 XRD pattern for films prepared by spray pyrolysis followed by sulfurization.....	63
Fig. 4.1 Absorption coefficient for iron pyrite versus photon energy.....	66
Fig. 4.2 Optical transmittance versus wavelength for a photoanode before (curve A) and after (curve B) use in solar cell.....	69
Fig. 4.3 Optical transmittance of electrolyte versus wavelength.....	71
Fig. 4.4 Optical transmittance of cell container versus wavelength.....	73

Fig. 4.5 I-V characteristic curve for a photoelectrochemical solar cell with photoanode A on illumination.....	75
Fig. 4.6 I-V characteristic curve for a photoelectrochemical solar cell with photoanode B on illumination.....	77
Fig. 4.7 Photoelectrochemical solar cells' response to wavelengths of varying energies.....	83
Fig. 4.8 Photocurrent density steadiness variation with time for photoelectrochemical solar cell.....	85

## LIST OF SYMBOLS

A	Area
$a_{\text{ox}}$	Concentration of oxidizing agent
$a_{\text{red}}$	Concentration of reducing agent
c.b	conduction band
d	Distance
e	Electron charge
$E_c$	Bottom of conduction band
$E_f$	Fermi level
$E_{f,\text{redox}}$	Fermi energy of redox system
$E_f^{\circ}$	Fermi level of redox system in vacuum
$E_g$	Energy band gap
$E_v$	Top of valence band
FF	Fill Factor
h	Planck's constant
I	Current
$I_m$	Maximum current output
$I_{sc}$	Short circuit current
k	Boltzman's constant
n	Electron concentration

$N_c$	Effective density of states in the conduction band
$N_d$	Concentration of donors
$nE_f$	Fermi energy for electrons
$nE_f^*$	Fermi energy level of electrons on illumination
$n_0$	Concentration of electrons at equilibrium
$N_v$	Effective density of states in valence band
$p$	Hole concentration
$P_{in}$	Illumination intensity incident on the cell
$P_m$	Maximum power output
$p_0$	Concentration of holes at equilibrium
PEC	Photoelectrochemical
$pE_f$	Fermi energy for holes
$pE_f^*$	Fermi energy of holes on illumination
$R_L$	Load resistor
$T$	Absolute temperature
$T_{1/2}$	Transmission ratio
$U_{redox}$	Redox potential
$V_m$	Maximum voltage output
$V_{oc}$	Open circuit voltage
v.b	valence band
$W_{ms}(0)$	Work function for electron emission from electrode to solution with electrode potential taken as zero
$W_{ms}(\phi)$	Work function at potential $\phi$

$\alpha$	Absorption coefficient
$\Delta G$	Energy level of electron
$\Delta G^{\circ}$	Energy level of electron in vacuum
$\Delta m$	Change in mass
$\Delta n$	Increase in electron concentration due to illumination
$\Delta_n E_f$	Change in Fermi energy level due to increase in electron conduction
$\Delta p$	Increase in hole concentration due to illumination
$\Delta_p E_f$	Change in the Fermi energy due to increase in number of holes
$\Delta t$	Thickness
$\epsilon$	Permittivity of media
$\epsilon_0$	Permittivity of free space
$\eta$	Efficiency
$\lambda$	wavelength
$\mu$	Carrier mobility
$\nu$	Photon frequency
$\rho_0$	Density
$\phi$	Potential
$\Phi$	Work function

N.B: Photoanode A - not-vacuum-annealed

Photoanode B - vacuum-annealed

UNIVERSITY OF NAIROBI  
CHROMO LIBRARY



## ABSTRACT

Iron pyrite, also known as iron disulfide, has been classified as one of the most promising materials for both thin film and photoelectrochemical (PEC) solar cells. In this study, iron pyrite was grown on tin oxide coated glass substrate. Iron oxide was first grown by spray pyrolysis and then sulfurized to convert the iron oxide into iron pyrite. The deposition parameters were optimized. Iron pyrite was characterized with respect to its optical and structural properties. Finally, a PEC solar cell was fabricated with iron pyrite as photoanode.

The optimized deposition parameters were: spray rate  $\approx 14$  ml/min, substrate temperature  $\approx 370.0$  °C for iron oxide and  $420.0$  °C for tin oxide, spray distance 30-35 cm. Annealing the iron oxide in sulfur vapour was done with the following optimized parameters: heating rate  $4-5$  °C/min, up to a temperature of  $350.0$  °C, cooling rate of  $1-2$  °C/min down to below  $80.0$  °C. The sample was then dipped in carbon disulfide and rinsed with distilled water.

Optical studies of iron pyrite gave an absorption band edge of about  $1.0$  eV, and an absorption coefficient in the range of  $10^4$  cm<sup>-1</sup>. The thermoelectric effect measurement failed to show whether the films were clearly n or p type. However, the current direction in the PEC solar cell indicated the films to be n type.

The PEC solar cell gave a short circuit current density of about  $40.0$   $\mu\text{A}/\text{cm}^2$  and an open circuit voltage of about  $64.5$  mV for a vacuum-annealed photoanode and  $2.4$   $\mu\text{A}/\text{cm}^2$  (short circuit current density) and  $11.0$  mV (open circuit voltage) for a non-vacuum-annealed photoanode. The efficiency of the vacuum annealed photoanode was  $2.71 \times 10^{-4}\%$  while that of the non-vacuum annealed photoanode was  $1.83 \times 10^{-6}\%$ .

# CHAPTER ONE

## 1 INTRODUCTION

The great and growing demand for energy has caused great importance to be attached to the exploration of new sources of energy. Solar energy is one of the major areas of new energy exploration.

The solar age promises to slow our dependence on the increasingly expensive, scarce and environmentally unfriendly fossil fuels and nuclear energy. The materials and principles involved in solar energy generation are intrinsically more manageable than those associated with large scale nuclear reactions. Solar energy represents an inexhaustible energy resource that can be utilized to supply man's energy needs for all time. The land required to provide all our energy needs is a small fraction of the land area required to produce food, and moreover, the land best suited for collecting solar energy is the land least suited for other purposes [Williams, 1977].

Solar energy's most attractive aspects include its comparative simplicity, benign nature, diversity and the promise of a lessened dependence on other sources of energy. For several years now, there has been considerable hope and keen interest centered on the development and fabrication of photoelectrochemical (PEC) solar cells due to their several advantages over the use of solid state cells. These advantages include their being: (i) easy and simple to make (ii) insensitive to gross defects (iii) low cost of manufacturing compared to p-n

junction solar cells (iv) large single crystals are not necessarily to be grown (v) p-n junction forms spontaneously on the semi-conductor making contact with the electrolyte (vi) no need for front metallization as in p-n photovoltaic solar cells (vii) no need for a transparent epitaxial layer [Lokhande and Dhumre, 1993; Heller and Miller, 1980].

The basic setup of these devices is the illumination of a semi-conductor electrode in an electrolyte. At the semi-conductor liquid junction, reduction takes place while oxidation takes place at the counter electrode-liquid junction. This happens for a p type material. The reverse is true for an n type material. This process continues with no net change in the electrolyte since a reduction in one electrode is counteracted by oxidation in the other. This leads to electric power generation when the two electrodes are connected via a load.

One of the most recent candidates and a potential material for solar energy production is iron-disulfide. It is a new solar material currently under active research [Ennaoui. et al, 1986; Ferrer and Sanchez, 1991; Hopfner et al, 1993; Fleming, 1988; Birkholz et al, 1990]. It has several advantages compared to other materials. These include:(i) material elements which are cheap, abundant and non toxic (ii) the energy gap of approximately 1.0 eV is sufficient for solar energy applications . (iii) its absorption coefficient (in the range of  $10^5/\text{cm}$  for  $h\nu > 1.3 \text{ eV}$ ) makes it attractive for use in both PEC and thin film solar cells [Ennaoui. et al, 1985] (iv) high electron mobilities

( $230 \text{ cm}^2 (\text{V}\cdot\text{S})^{-1}$ ) good for electrical conduction [Shuey, 1975] (v) the high contribution of d-states to the valence energy band is very important in PEC applications, thus pyrite promises to be of good stability in terms of corrosion [Tributsch, 1982] (vi) high quantum efficiencies (approximately 90%) in I/I solution [Ennaoui, 1985].

A number of researchers [Ennaoui et al, 1986; Ennaoui and Tributsch, 1984] have used iron pyrite as a photoelectrode in the design of PEC solar cells. The results have been encouraging and there are indications of a bright future for PEC solar cells.

One of the major drawbacks of photoelectrochemical (PEC) semi-conductor devices is the chemical instability of the semi-conductor electrodes. Suggestions like the use of cycle-based reversible redox reactions of eg. sulfur on cadmium sulfide semi-conductor electrode have been tried [Bolton, 1977]. The use of polysulfides has also been suggested [Backus, 1977]. The polysulfides actively participate in fast electron transfer processes or even precipitate on the electrode surface and thus improve the stability of the light sensitive surface. However, these suggestions and techniques are only applicable for a short period of time and do not represent a long term solution to the instability problem. Conceptually, we will have achieved a great deal by the manufacture of stable photoelectrochemical devices. The present study involved and accomplished the following study objectives: (i) the growth of iron disulfide thin film on a glass substrate by spray pyrolysis (ii) the

optimization of deposition parameters in an endeavor to grow good films (iii) characterization of the prepared iron disulfide film, (iv) use of iron disulfide as a photoelectrode in a photoelectrochemical (PEC) solar cell studies. Spray pyrolysis as a thin film growing technique was used due to its low cost and suitability for large scale film production.

## 1.1 LITERATURE REVIEW

This section is devoted to the general review of the work researchers have done as regards to photoelectrochemical solar cells. This is quite a new field of research in search for other forms of energy along side solid state devices. Discussion is made of the different types of photoelectrochemical solar cells that have been tried and the shortcomings of the these types of solar cells.

### 1.1.1 The *Photoelectrochemical solar cell*

Solid-liquid junction solar cells can be classified into three:

- a) photoelectrochemical (PEC) solar cells
- b) photoelectrolysis solar cells.
- c) photogalvanic solar cells

In the PEC solar cell first pioneered by Fujishima and Honda [Fujishima and Honda, 1972] there was no net chemical reaction in the electrolyte for oxidation at one electrode was accompanied by reduction at the other. Thus only electric current was generated. Conversion of light energy into electrical by the use of photoelectrochemical solar cell is through the semi-conductor-electrolyte interface. The photoelectrolysis solar cell comprises photoelectron decomposition of water i.e optical energy is converted into chemical energy. Thus hydrogen and oxygen are liberated at the electrodes [Bolton, 1977; Fujishima and Honda, 1972; Tokio, 1979 ]. In photogalvanic solar cells,

molecular species in solution absorb the incident light and electrical power is generated by charge transfer from excited species to the electrodes in contact with light absorbing system.

## *2 Progress in semiconductor-liquid junction solar cells*

A lot of research on iron-disulfide as a solar cell material has been done and solar energy conversion efficiencies of the order of 1% and lower for  $I^-/I_2$  synthetic  $FeS_2$  under an illumination intensity of  $800 \text{ mW/cm}^2$  have been reported [Ennaoui and Tributsch, 1984]. Further, they obtained a straight line graph power output curve with a negative temperature gradient. This indicated a poor value for the fill factor, a low photovoltage and a high series resistance. The cell had an average quantum efficiency of 33% with visible Xenon light (intensity  $40 \text{ mW/cm}^2$ ). However, the cell did not show any decay within a twenty four hour period.

Later Ennaoui and others [Ennaoui et al, 1986] attempted to fabricate a PEC solar cell with  $0.5 \text{ M Na}_2\text{SO}_4$  as electrolyte under an illumination of  $4\text{-}5 \text{ W/cm}^2$ . They observed a relatively high dark anodic current ( $10 \text{ mA/cm}^2$ ) at  $1.0 \text{ v}$ . A significant anodic corrosion was also observed.

They tried other electrolytes such as:  $S^{2-}/S_n^{2-}$ ,  $Fe(CN)_6^{3-/4-}$ ,  $Fe^{2+/3+}$ ,  $Br^-/Br_2$ ,  $Cl^-/Cl_2$  and  $Ce^{3-/4-}$ . A shift of the onset of photocurrents with the redox potentials for each electrolyte was observed. They attributed this behaviour to unpinning of energy bands (Fermi level pinning) by the presence of surface states. A redox solution of  $1.0 \text{ M CaI}_2$ ,  $4.0 \text{ M HI}$  and  $0.05 \text{ M I}_2$  under a  $4\text{-}5$

W/cm<sup>2</sup> illumination intensity by a W-halogen lamp with n-FeS<sub>2</sub> as photoanode gave a photocurrent density of between 1-2 mA/cm<sup>2</sup>. However, in this case the electrode was etched in an aqueous solution of 0.5 M H<sub>2</sub>SO<sub>4</sub>/H<sub>2</sub>O<sub>2</sub>(30%) mixed in the ratio of 1:1 [Ennaoui et al, 1986]. MoS<sub>2</sub> based PEC solar cells using non-aqueous solutions, have low efficiencies but good stability. An equivalent stability and high efficiency for MoSe<sub>2</sub> with a redox system of acetonitrile solution containing Cl<sup>-</sup>/Cl<sub>2</sub> can be obtained. With a single crystal of n-WSe<sub>2</sub> in iodide-triiodide redox solution and using a carbon counter electrode, Heller and Miller [Heller and Miller, 1980] report efficiencies of 10%. Furen and others [Furen et al, 1980] have reported an efficiency of 14% for the same system but using a platinum counter electrode and on replacement of the redox couple with bromide-bromine, the efficiency drops to 11%. The low absorption by Br<sup>-</sup>/Br gave a high short circuit current but a lower fill factor and open circuit voltage.

Chemically deposited CdSe films as photoelectrodes have also been used in PEC solar cells. Photocurrent values of 0.19 mA and photovoltages of 150.0 mV were measured with 1.0 M KI as electrolyte under an illumination intensity of 100 mW/cm<sup>2</sup> [Lokhande and Dhumre, 1992]. Other materials like n-Ag<sub>2</sub>S as electrodes in 1.0 M (NaOH-Na<sub>2</sub>S-S) electrolyte have been used [Lokhande and Dhumre, 1993]. The values for the photocurrent and photovoltage were 0.256 mA and 95.0 mV respectively.



### 1.1.3 *Semiconductor electrode materials for photoelectrochemical (PEC) solar cells*

One of the most studied semi-conductor electrodes is GaAs. Being a direct band-gap semi-conductor material, efficiencies obtained with it are as high as 19%. Its high cost is, however, a draw back. GaP with an energy band gap of about 2.23 eV is more suited for use in photoelectrolysis cells than in PEC due to this high energy gap. InP (1.3 eV) is likely to be unstable due to its low band gap. InP has also been mentioned as being sensitive to water vapour and thus not suited for solar cells [Boer and Piprek, 1994]. Efficiencies of 6.4% and 7.5% have been obtained with n-CuInS<sub>2</sub> and CuInSe<sub>2</sub> in polysulfide electrolyte [Weman *et al*, 1989; Lona, 1997]. The performance of a PEC solar cell depends on the preparation of the semi-conductor electrode. The characterization of such thin film electrodes is thus very important and structural, optical and electrical properties of such thin film electrodes are of paramount interest.

The main concern in the research is the studies of semi-conductor/electrolyte interface coupled with the development of efficient solar to electrical energy conversion systems and/or the production of chemical species from sunlight. It is the aim of researchers to discover inexpensive materials whose energy band gap matches that of solar spectrum and which are stable in operation. Promising candidates, according to Tributsch [Tributsch, 1982], are transition metal dichalcogenides. Their general

chemical formula is  $MX_2$ ; M being the transition metal atom and X one of the chalcogens either S, Se or Te. A total number of sixty exist in two classes: pyrite type and layered type. The layered type semi-conductors according to studies [Tribusch, 1982] show laboratory efficiency and good stability in redox solutions. Generally, elements in groups 4B and 6B columns show good semi-conducting properties.

#### 1.1.4 Draw backs of photoelectrochemical solar cells

The advantages of PEC solar cells over p-n junction photovoltaic cells would be of little use if reasonable efficiencies and stability cannot be achieved. As cited earlier, a 12% solar-to-electrical conversion efficiency has already been obtained [Miller and Heller, 1980]. Even with the efficiency of 12% so obtained by Miller and Heller, 1980, the photoanode electrode was still unstable.

The approach to solve the instability problem has assumed many dimensions. The selection of semi-conductor-redox couple solution pairs for which the self oxidation of semi-conductor is kinetically overcome has been suggested [Heller and Miller, 1980]. One method is to have redox couples with fermi level close to the conduction band i.e fermi level about 0.1-0.2 ev below the conduction band. However, excess reduction drops the cell voltage and efficiency significantly. By making the oxidation of the redox couple greater than that of the semi-conductor, the rate of

UNIVERSITY OF NAIROBI  
CHIRONGI LIBRARY

hole transport (semi-conductor oxidation) can also be reduced. Miller and Heller, 1980, have noted that the most stable semi-conductors to be used as photoanodes are those with large band gaps. This implies absorption spectra which poorly overlap the solar spectrum.

It has been suggested [Hovel, 1975] that since it is not possible to apply an anti-reflection coating at the semi-conductor-liquid junction, an alternative would be to build an appropriate surface roughness into the interface. In a PEC solar cell, the redox process competes well with the anodic dissolution when the energy states of the redox system are not located near the valence band but somewhat above it. This means that surface states, energy levels at the semi-conductor surface are involved. In this case electrons are first transferred from the redox system into these states and recombine with the holes created by illumination of the photoanode. Such surface states can occur as intermediate states in the photocorrosion reaction. Thus, holes move towards the surface and cause the breaking of a surface bond. The remaining unpaired electron is then no longer in the valence band state but in energy state situated above the valence band. As soon as another hole is trapped, the next bond may be destroyed and a surface group dissolved. Memming, 1980, has suggested that the formation of another hole can be prevented if an electron is transferred from a suitable redox system to a surface group at which one bond is already broken so that the bond is restored. Thus the stabilization consists of a partial

dissolution followed by a regenerative process.

Lokhande and Dhumre, 1993, have noted that since the photocorrosion is caused by accumulation of holes at the photoanode, hole scavengers (negative ions and other molecules that have high affinity for holes) can be introduced to neutralize the holes [Lokhande and Dhumre, 1993]. The scavenger concentration should always be high enough and the distance between the two electrodes should be small to increase the mass transfer rate. All the above suggestions have been tried in one way or the other and the results have been positive. Results obtained by Heller and Miller, 1980, related to instability of n-GaAs in 1.0 M KOH PEC solar cell whose photoanode was prepared by chemical deposition have been encouraging. Using CdSe as a hole-accepting ion, Heller and Miller, 1980, showed that the ratio of current going to corrosion to total current on increasing the hole-accepting ion concentration fell from 1.0 at 0.0 M hole-accepting ion concentration to about 0.01 at 0.2 M hole-accepting ion concentration. They also obtained a corrosion current reduction of about 30.0  $\mu\text{A}$  in an n-CdS in 1.0 M  $\text{Fe}(\text{CN})_6^{4-}/\text{Fe}(\text{CN})_6^{3-}$  solution PEC solar cell by making the rate of hole transport greater than the rate of self oxidation of the illumination semiconductor.

Investigations by Lokhande and Dhumre, 1993, have shown that a mixture of 1.0 M KCl and 1.0 M NaCl in the ratio 1:1 improved the stability of PEC solar cells formed with CdSe electrodes to 120 minutes; compared to 50 minutes in the absence of the

chloride solutions. The photoelectrode was prepared by chemical deposition. Lokhande and Dhumre, 1993, have also prepared  $\text{Ag}_2\text{S}$  anodes but used them in various charge storage configurations. The results indicated the possibility of storing chemical energy by using chemically deposited  $\text{Ag}_2\text{S}$  and  $\text{CdSe}$ .  $\text{Ag}_2\text{S}$  in 1.0 M polysulfide gave a short circuit current of 0.129 mA and an open voltage of 15.0 mV on charging whilst on discharging it gave 0.044 mA as the short circuit current and 5.0 mV as open voltage.

## CHAPTER TWO

### 2 THEORETICAL BACKGROUND

#### 2.1 Introduction

The history of the studies of the photovoltaic phenomena at electrode-electrolyte dates back over hundred years. Becquerel in 1879 detected electric currents when one of the identical electrode immersed in dilute acid solutions was illuminated. The immense work that followed made it possible in 1887 for the discovery of the electron photoemission effect at the electrode interface. This consists of the absorption of a light quantum by the electrode releasing electrons into the electrolyte in partially free form. The photoemission of electrons drew great attention and has been the object of intensive research both in experimental and theoretical aspects [Bolton, 1977]. The results obtained influenced a great deal the development of quantum theory of light, solid state physics and other problems of modern physical sciences. There has been great diversity in the photosensitive electrochemical systems development and a large class of theories to explain the generation of the photo response in such systems.

Photocells can be classified into three major groups depending on processes taking place in them. The first group comprises of systems in which the photocurrent is generated due

to absorption of light by the solution leading to homogeneous photochemical reactions. The current variation at the electrode is caused by the formation of excited molecules, free radicals or other photolysis products that might undergo reduction or oxidation at the electrode. The electrode simply acts as a detector for the photochemical reactions and does not take part in the photo process. The second group is that of the photo process that take place on semi-conductor electrodes. The inner photo effect i.e, generation of minority current carriers in the semi-conductor (electrons in the conduction band, holes in the valence band) is responsible for the photocurrent in this case. The final group consists of photovoltaic systems consisting of metals with a clean surface in contact with a non-absorbing electrolyte.

There are three possible mechanisms for the photocurrent generation in the third group suggested by Sihvonen [Sihvonen, 1977]: (i) emission of electrons from the metal into the solution in the presence of light (ii) photodischarge of dissolved species and (iii) decomposition of adsorbed molecules under the action of light with the formation of cations and anions on the surface. The cations and anions ultimately pass into the solution.

Experiments [Cheremisinoff and Regon, 1978] conducted with alkali metal amalgam in aqueous solution suggest that the rate of decomposition of the metal in solution depended on the light polarization. The reaction rate was faster when the electric field vector was normal to the metal surface as compared to when

it was parallel. This suggests the possibility of the photoemission passing from the metal into solution. The three outlined mechanisms of photo current generation are not mutually exclusive though one may be predominant depending on the experimental conditions.

## *2.2 Design of a photoelectrochemical solar cell*

The change in the electrode potential (on open circuit) or in the current flowing in the external circuit (under short circuit conditions) of an electrode/electrolyte system on irradiation is termed as photoelectrochemical effect.

For generation of power from a semi-conductor/electrolyte junction, the semi-conductor has to be combined with a suitable counter electrode in what is termed as a galvanic cell (see Fig. 2.1).

UNIVERSITY OF NAIR  
CHIROMO LIBRARY



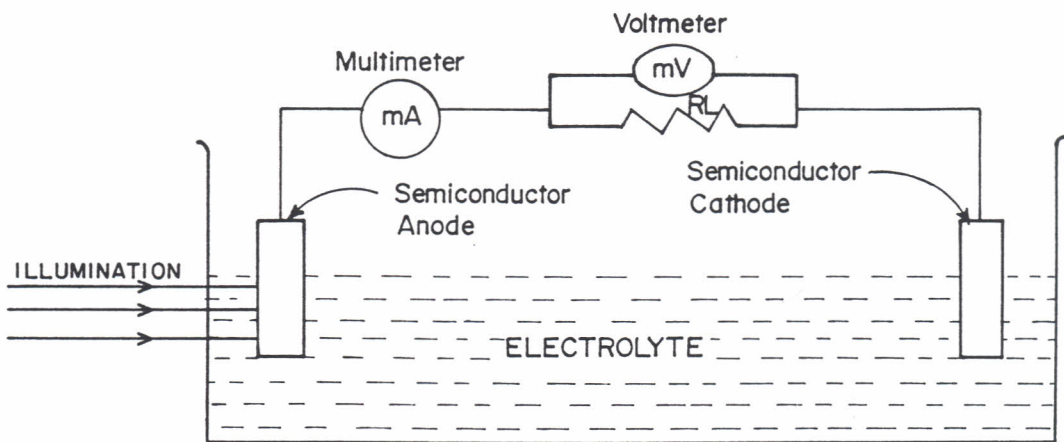


Fig. 2.1 Schematic diagram of a photoelectrochemical (PEC) solar cell.

Heller and Miller have argued that a 12% solar-to-electrical conversion efficiency is possible with PEC solar cells [Heller and Miller, 1980]. Problems associated with achieving stable and efficient solar cells spring from electrolyte exposed semi-conductor surface. This introduces photocorrosion, light induced ion exchange, interfering surface states, impurities, and prevention of non-reflecting coating being applied. The semi-conductor liquid junction solar cell (Fig.2.1) can be viewed as a battery functioning when one of the electrodes is illuminated [Gerischer, 1978; Williams, 1977] consuming photons only but not the cell material.

The reaction equation in Fig.2.1 is given as:

At anode



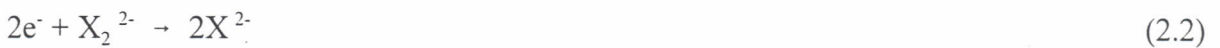
where

$h^+$  is a hole

$x^{2-}$  is reduced species

$x_2^{2-}$  is oxidized species

At cathode



where

$e^-$  is the electron

$x_2$  is reduced species

$x_2^{2-}$  is oxidised species

The electrochemical potential of electrons is represented in solids by their Fermi level and in redox couple solutions by the Nernst potential. When a semi-conductor gets into contact with a solution, there is equalization of the redox potential and the semi-conductor's Fermi level resulting in bending of the conduction and valence bands as shown in Fig.2.2 [Sihvonen in Bolton, 1977].

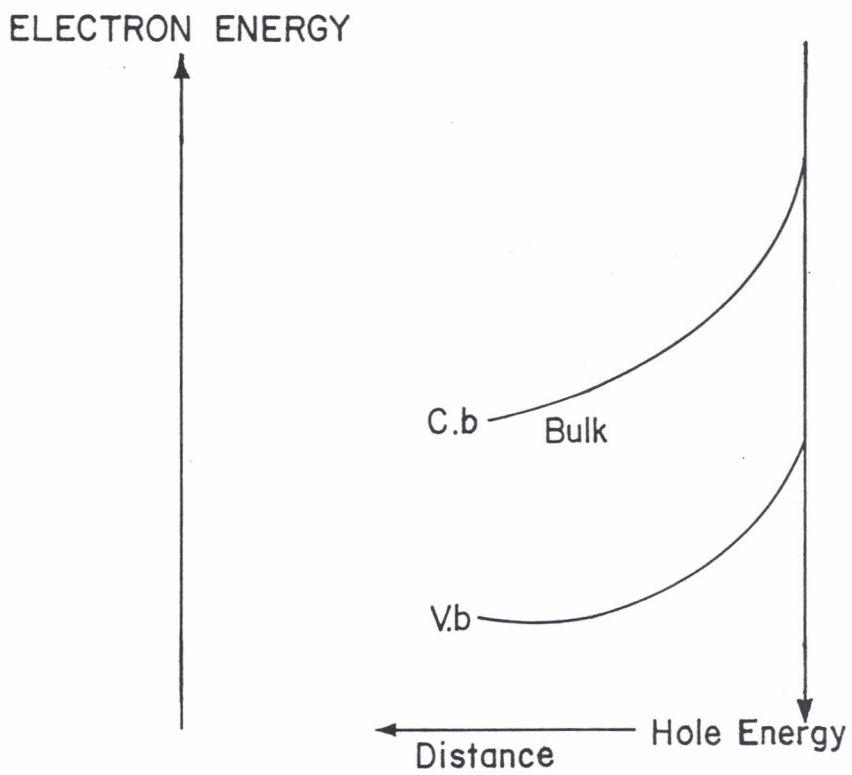


Fig. 2.2 Band shapes in the bulk of an illuminated n-type semiconductor .

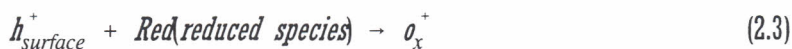
The extent of bending approximates the difference between redox couple potential and the Fermi level of the semi-conductor representing the barrier height. This is the limit of the achievable cell voltage and also implies potential gradient or electric field at the interface. Photoexcitation of electrons from valence to conduction bands is followed by separation of holes and electrons in this field. The hole-liquid interface oxidizes the member of redox couple and electrons move through the bulk of semi-conductor and back contact to external load. The electrons finally reach the cathode and the redox couple is reduced. For good cells therefore, anode and cathode reactions should be equal and opposite.

The natural counter electrode for a semi-conductor/redox electrolyte system is a reversible redox electrode for the same redox system. The same redox potential controls the equilibrium at both the electrodes, the Fermi levels being equal in both the solid and the electrolyte. The counter electrode provides the further advantage that it guarantees a rapid attainment of equilibrium at the semi-conductor electrode after bringing both electrodes into electronic contact, as the time constant in this case is controlled by the double layer capacity and the external resistance instead of the interfacial electron transfer resistance.

Under illumination, the photovoltage drives the electron from the semi-conductor to the counter electrode, while the holes react with the electrolyte. As a result the oxidation of Red

(reaction (2.3) below) at the semi-conductor electrode is compensated by the reduction of  $O_x^+$  at the counter electrode (reaction (2.4) below) [Bolton, 1977]. In this case, no net chemical change occurs.

Interfacial reactions:



The maximum open circuit voltage that can be generated is equal to the amount of band bending and is therefore controlled by the electrolyte Fermi level for a given semi-conductor. The operational efficiency of the photoelectrochemical (PEC) Solar cell depends on the relative rates of electron-hole recombination and electron transfer. Several energy loss mechanisms are operative in solid junctions. These include: (i) energy loss as charge carriers cross the space charge layer (ii) Ohmic losses (iii) energy loss due to oxidation of Red at the semi-conductor

electrode (iv) energy loss due to reduction at the counter electrode. For better performance, one has to minimize: (i) energy losses in the cell circuit (ii) light losses caused by absorption outside the space-charge layer in the electrolyte and by reflection.

Photodecomposition of the semi-conductor imposes another restriction on the extent of band bending. To prevent photodecomposition, the Fermi level of the redox system in the electrolyte must not exceed the decomposition Fermi level of the semi-conductor for the particular reaction with the minority carriers. The further the redox Fermi level of the electrolyte is below the anodic decomposition Fermi level of n-type material, or (above the anodic decomposition Fermi level for p-type material), the greater the risk of photodecomposition. The distance between the two electrodes has to be as small as possible to minimize concentration differences. Stirring also helps in achieving efficient rates by convection. The electrolyte layer between the photoelectrode and the counter electrode should be kept thin.

The electrolyte containing the redox couple must be transparent to the useful wavelength of the incident light so that maximum light intensity is incident at the depletion layer from front. The semi-conductor photoelectrode, the electrolyte and the counter electrode should be arranged in a configuration optimum for uniform current distribution in the cell.

### 2.3 Processes at Semiconductor electrolyte boundary

Just as metal electrodes, semi-conductor electrodes can undergo redox reactions by electron transfer between the electrode and the redox system in solution. However, a chief difference is the existence of a band gap in the energy distribution of electron states in semi-conductors. The electron transfer occurs within the two bands, conduction and valence and depends on whether it occurs via the conduction or valence, the type of semi-conductor and the specific redox system. This is due to the electron transfer occurring between the electron energy states of the same energy, one occupied and the other empty. A redox reaction at the semi-conductor comprising holes and electrons is thus [Bolton, 1977]:



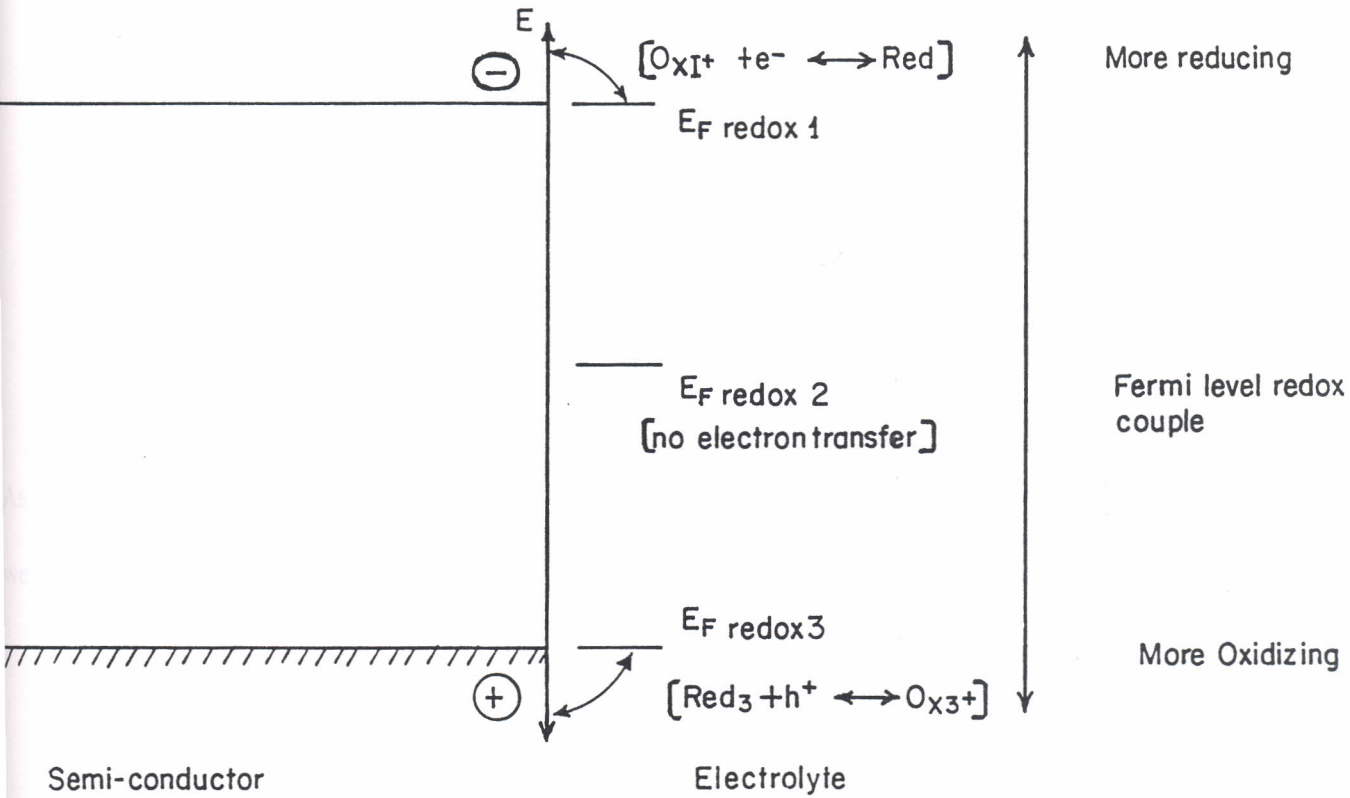
or



The importance of the energy positions of band edges and redox species is shown below in Fig.

2.3 [Bolton, 1977].





3 Energy relations between semiconductor and redox couple in solution controlling electron exchange.

The standard redox potential ( $U_{\text{redox}}$ ) and re-organization energy characterize the electronic energy states in solution. There is need to introduce an absolute scale for the equilibrium potentials of the redox systems in solution for comparison and the adjustment to the models of solid state physics. This is done by taking the vacuum level of electrons as the reference energy rather than the hydrogen electrode in aqueous solution [Bolton, 1977].

A formulation for a redox reaction is thus for an electron transfer between vacuum level and vacant states in solution:



where

$\Delta G$  = Energy level of electron

$\Delta G^0$  = Energy level in vacuum

Assuming that the electron is at the energy level corresponding to  $\Delta G^0$  instead of vacuum level, then we have at equilibrium of reaction  $\Delta G = 0$  - the Fermi energy  $E_f$ .

$$E_{f,\text{redox}} = \Delta G^0 = E^0_{f,\text{redox}} + kT \ln\{a_{\text{red}}/a_{\text{ox}}\} \quad (2.8)$$

where

$E_{f,\text{redox}}$  is Fermi energy of redox system

$E_f^0$  is Fermi energy of redox system in vacuum

$a_{\text{red}}$  is concentration of reducing agent

$a_{\text{ox}}$  is concentration of oxidizing agent

$k$  is Boltzman's constant

$T$  is absolute temperature

We relate the absolute scale of Fermi energies and the electrochemical redox potential scale  $U_{\text{redox}}$

by [Bolton, 19977]

$$E_{f,\text{redox}} = -eU_{\text{redox}} + E_f^0 \text{ (ref. electrode)} \quad (2.9)$$

where

$e$  is electronic charge

$U_{\text{redox}}$  is the redox potential

For the description and understanding of the thermodynamics of redox reactions between electrons in conduction band (c.b) or holes in valence band (v.b) and redox species in solution, we attribute individual redox potentials to each of the electronic transitions. Thus for electrons in the c.b we have

[Bolton, 1977]

vacant state in c.b +  $e^-_{\text{vac}} \rightleftharpoons e^-_{\text{c.b}}$

$${}_n E_f = E_c + kT \ln \{n/N_c\} ; \text{ for } n \ll N_c \quad (2.10)$$

where

$E_c$  is lower edge of conduction band

$n$  is electron concentration

$N_c$  is effective density of states in conduction band

$k$  is the Boltzmann's constant

$T$  is the absolute temperature

${}_nE_f$  is the Fermi energy for electrons

Similarly for holes in valence band,

$h^+_{v.b} + e^-_{vac} \neq$  occupied state in v.b

$${}_pE_f = E_v - kT \ln\{p/N_v\} \quad (2.11)$$

where

$E_v$  is the upper edge of valence band

$p$  is concentration of holes

$N_v$  is effective density of states in v.b

$k$  is Boltzmann's constant

$T$  is the absolute temperature

${}_pE_f$  is Fermi energy of holes

In equilibrium, the Fermi level of electrons and holes coincide due to the equilibrium condition

[Bolton, 1977]:

$$n_0 p_0 = N_c N_v \exp\{(-E_c - E_v)/kT\} \quad (2.12)$$

obtained since

$${}_nE_f = {}_pE_f ; \text{ for } n = n_0, p = p_0 \quad (2.13)$$

UNIVERSITY OF NAIROBI  
CHIRONGI LIBRARY

where

$n_0$  is concentration of electrons at equilibrium

$p_0$  is concentration of holes at equilibrium

## 2.4 Interface of semiconductor-electrolyte

When a semi-conductor is brought into contact with an electrolyte containing a redox system equilibrium is attained by electron exchange at the interface. At equilibrium, the Fermi levels are adjusted by the formation of an electric double layer between the electrolyte and the semi-conductor; the structure which depends mainly on the concentration of the mobile and the immobile charge carriers on both sides of interface.

If a semi-conductor is in contact with an electrolyte, a depletion layer develops as a consequence of the mismatch of the Fermi level  $E_f^\circ$  of the semi-conductor and the Fermi level  $E_{f\_redox}$  of the electrolyte. At equilibrium, the band bending is energetically equal to the initial difference in the Fermi levels. At the particular redox potential of the electrolyte, when  $E_{f\_redox} = E_f^\circ$ , there is no excess charge in the semi-conductor and hence no band bending. The bands are thus flat from the bulk to the surface and the corresponding redox potential is referred to as flat band potential,  $V_{FB}$ . The value of  $V_{FB}$  depends on the properties of the semi-conductor, the chemical nature and the doping concentration control  $E_f^\circ$  and the composition of the electrolyte.

When a semi-conductor is used as an electrode in an electrolyte a variable electric charge can then be accumulated in the space charge region underneath the interface with the electrolyte by the application of a voltage. Thus the concentrations of charge carriers and band edge energy values differ between the surface of semi-conductor and bulk. We concentrate on their values at the surface.

The exact position of the band edges in contact with an electrolyte depends entirely on the semi-conductor and composition of the electrolyte. Capacity measurements in a potential range where a depletion layer is formed underneath the semi-conductor surface can be obtained experimentally. It is possible to apply the space charge theory and extrapolate from the above measurements and get the flat band condition or potential. There are no excess charges found in the space charge layer of the semi-conductor. Under such a situation, the band edge in the bulk and the surface coincide. The Fermi-level in the bulk of semi-conductors is controlled by the applied potential and the energetic position of the band edges at the surface against the electrolyte can be calculated. The variation of band edge position in the surface with the applied electrode potential is very small due to the large voltage drop in the space charge layer of the semi-conductor and the little effect of applied potential on the Helmholtz double layer at the semi-conductor electrolyte interface. However, the double layer is a function of the electrolyte position.

The electrolyte effect is due to either ion adsorption or dissociation of ionic components from semi-conductor surface. The ionic double layer formation by the strong interaction between ions in solution and semi-conductor surface gives a method of varying the redox potentials of electrons and holes in semi-conductor relative to redox systems in solution. The existence of electronic surface states at the semi-conductor complicates things. The surface states may either be filled or emptied in a certain range of polarization of the electrode depending on their energy positions, a process that changes the potential drop in the Helmholtz double layer similar to ion adsorption [Gerischer and Tobias, 1978; Weman, 1989; Bolton, 1977; Bockris, 1959].

## 2.5 The effect of illumination

Electron-hole pairs are generated when light of energy  $h\nu \geq E_g$  (band gap of semi-conductor) falls on the semi-conductor surface after crossing the transparent electrolyte layer. If carriers are generated in the space-charge layer, they move in opposite directions as a result of the electric field in the layer. Assuming no recombination, the majority carriers migrate to the bulk and the minority carriers to the surface. Thus n-type semi-conductors act as photoanodes and dark cathodes while p-type materials act as photocathodes and dark anodes. For n-type semi-conductor electrodes in an ideal case, the holes react at the interface exclusively with the electrolyte, oxidizing the donors (Red) of the redox system.

The difference in the thermodynamic properties of holes and electrons for circumstances far from equilibrium is very vital. The steady state is attained when the generation is equal to annihilation of holes and electrons and the concentration increase by  $\Delta n$  and  $\Delta p$  with some distribution in space. The individual redox potential of electrons and holes effective at the electrode in the steady state of illumination or quasi-Fermi energies  $E_f^*$  is obtained by putting the value at the surface for  $n + \Delta n$  in (2.10) and  $p + \Delta p$  in (2.11). Equation (2.12) becomes invalid since  $n$  is no longer equal to  $n_0$ , and  $p$  to  $p_0$ . The shift of quasi Fermi level of holes and electrons is given by equations (2.10) and (2.11) in the form:

$${}_n E_f^* = {}_n E_f + \Delta {}_n E_f \quad (2.14)$$

and

$$\Delta {}_n E_f = kT \ln \left\{ \frac{(n_0 + \Delta n)}{n_0} \right\} \approx kT \ln \left\{ \frac{\Delta n}{n_0} \right\}; \text{ for } \Delta n \gg n_0 \quad (2.15)$$

where

${}_n E_f^*$  is Fermi energy level of electron on illumination

${}_n E_f$  is Fermi energy level of electrons in dark

$\Delta {}_n E_f$  is change in Fermi energy level due to increase in electron conduction.

$\Delta n$  is the increase in electron concentration due to illumination

$n_0$  is the initial concentration of electrons at equilibrium



$${}_pE_f^* = {}_pE_f + \Delta {}_pE_f \quad (2.16)$$

$$\Delta {}_pE_f = -kT \ln[(P_o + \Delta P)/P_o] \approx -kT \ln[\Delta P/P_o];$$

$$\text{for } \Delta p \gg P_o \quad (2.17)$$

where

${}_pE_f^*$  is the Fermi energy of holes on illumination

${}_pE_f$  is the Fermi energy of holes

$\Delta {}_pE_f$  is the change in the Fermi energy due to increase in number of holes

$\Delta p$  is the increase in hole concentration due to illumination

$p_o$  is the initial concentration of holes at equilibrium

In well conducting semi-conductors,  $n_o \gg p_o$  or  $p_o \gg n_o$  thus from above equations, a shift in quasi Fermi level is possible for minority carriers. Using the above equations, it is easy to estimate the maximum free energy which can be gained from an illuminated semi-conductor electrode.

On the surface of a semi-conductor electrode, the excess concentration of minority carriers depends on (i) light intensity (ii) absorption coefficient (iii) quantum yield for electron-hole pair formation (iv) recombination rate in the space charge layer (v) transport phenomena. The band bend in the space charge layer is reduced drastically at saturation and the potential

distribution close to that of the flat band situation.

Our discussion has been on inert material semi-conductor electrodes capable of exchanging electrons and holes with a redox system in an electrolyte. We have very few such semi-conductors. A large class of semi-conductors can undergo reduction due to an accumulation of electrons in the conduction band or oxidation due to accumulation of holes in the valence band and in turn form soluble or insoluble products. This reactivity is a major obstacle to the use of semi-conductors in photoelectrochemical cells e.g cadmium sulfide is oxidized into  $\text{Cd}^{2+}$  ions and sulfur molecules, zinc oxide into  $\text{Zn}^{2+}$  ions and oxygen molecules by holes generation to the surface [Peter, 1978; Bolton, 1977]. Some materials can be reduced by electrons of the conduction band to cadmium metal and  $\text{S}^{2-}$  ions or zinc and  $\text{OH}^-$  ions respectively. These reactions have the effect of :

- i) changing the properties of materials
- ii) production of surface films by catalyzing recombination processes between holes and electrons
- iii) blocking current flow
- iv) absorbing a lot of light to make electrode inefficient for energy conversion.

However, titanium dioxide is stable to these decompositions, but the band gap is too wide for it to give some good efficiency.

## 2.6 Photoemission into electrolyte

This is the first stage of a complex multi-step process compared to the photoemission of electrons from metal to vacuum. It comprises three stages:

- a) transition of electrons through the interface after absorption of a light quantum.
- b) thermalization and solvation of the emitted electrons. This leads to a reduction in their initial energy to the level of thermal kinetic energy and formation of solvated electrons. This takes a very short time, in the order of  $10^{-9}$  s.
- c) The electrons formed in solution enter into chemical reaction with solutes being capable of reacting with electrons e.g  $\text{H}_3\text{O}^+$ ,  $\text{NO}_3^-$ , or  $\text{N}_2\text{O}$ ,  $\text{O}_2$ ,  $\text{CO}_2$ . These solutes and molecules, capable of capturing electrons are termed as electron scavengers [Beda *et al*, 1987; Bolton, 1977].

In the event of non-existence of electron scavengers, solvated electrons return to the electrode at a rapid rate, the result is a stationary photocurrent in the system i.e zero photocurrent. This is because there is no electron transfer from one electrode to the other in the electrolyte. The electron scavengers can react with solvent molecules, however, the rate of reaction is so small that no noticeable rise in photocurrents is obtained.

The existence of an electrical double layer at the electrode-electrolyte interface makes all the external potential applied to the electrode concentrate here thus an additional photoemission parameter, electrode potential comes into existence. Assuming the ohmic potential difference drops across the electrolyte in strong electrolyte, the potential remains practically constant outside the dense part of the double layer. If a potential  $\phi$  is applied to the system, the energy level of an electron in solution at a distance which exceeds the double layer thickness changes by  $e\phi$ . Thus the electron work function changes:

$$W_{MS}(\phi) = W_{MS}(0) + e\phi \quad (2.18)$$

where  $W_{ms}(0)$  = work function for electron emission from electrode to solution with electrode potential taken as zero;  $W_{ms}(\phi)$  = work function at potential  $\phi$ ;  $e$  = electronic charge.

The electrons in photoemission into the electrolyte fall in a condensed medium (electrolyte) gaining energy due to electron-medium interaction. The nature of movement of the electrons in the electrolyte is quite different from that in vacuum. The electrons emitted into the electrolyte enter into collective interaction with the solvent and solute molecules. It is postulated that the image forces in the electrolyte are partially or even totally screened by the ions in the solution [Gerischer and Tobias, 1978; Roy et al, 1986; Bolton, 1977]. It is important to note that photoemission into electrolyte can only be

UNIVERSITY OF NAIROBI LIBRARY

observed when the electrolyte contains electron scavengers. Further, the solvated electrons undergo a chemical reaction with the scavenger for the existence of the stationary photocurrent. Thus photoemission assumes an electrochemical reaction.

## 2.7 Charge separation by electric field in the semiconductor

Charge carriers of opposite sign can be separated more efficiently if the light absorption occurs in a range where an electric field is present. This seems only possible in the space charge layer of semi-conductor electrode more so, in the depletion layers in which excess charge is formed by immobile donors or acceptors. The excess charge of a semi-conductor electrode depends on the applied potential. A positive excess charge is needed for an n-type semi-conductor and a space charge layer depleted of electrons is formed at potentials positive from the flat band potential. A p-type semi-conductor has a space charge layer depleted of holes at a potential negative from the flat band potential. This can be achieved by: the application of external voltage against a suitable counter electrode or immersion of the electrode into a suitable redox system electrolyte (see Fig.2.4) [Bolton, 1977; Sihvonen:in Bolton, 1977].

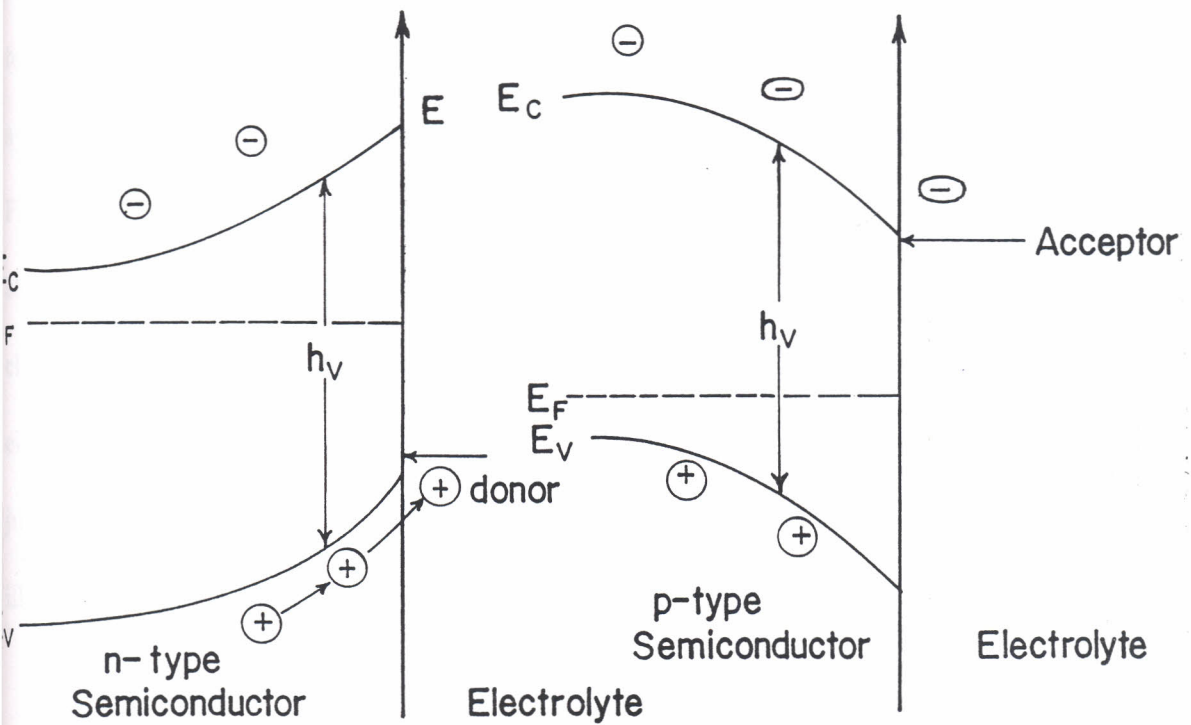
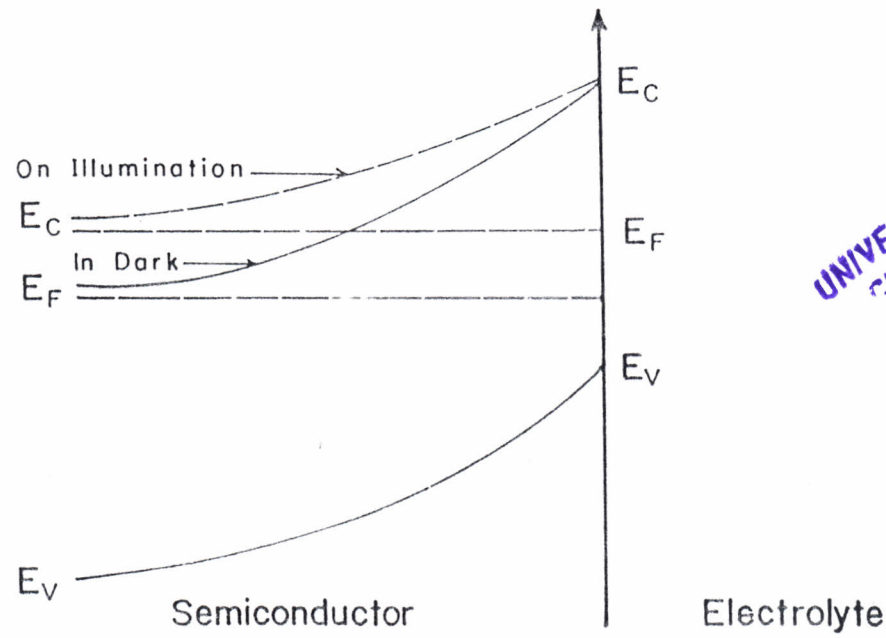


Fig. 2.4 Effect of illumination in depletion layer and electron transfer reaction at semiconductor-electrolyte interface.

The immersion of an electrode into a suitable redox electrolyte system is analogous to a heterojunction in solid state devices. On illuminating, the depletion layer electron-hole pairs are generated [Bolton, 1977]. These are separated by the electric field present in this layer driving the minority carriers to the surface and the majority to semi-conductor bulk. The probability of recombination is minimized. The rate of recombination depends on (i) presence of traps in the space charge layer (ii) cross-section for recombination of holes and electrons (iii) field strength.

The charge separation process causes a disturbance of the electric field present in the space charge. To counter this change in electric field in the space charge, another field acts as a driving force for electrolysis between the semi-conductor electrode and a counter electrode. Thus there is a shift in the Fermi-level in the semi-conductor bulk relative to the energy level in solution (see Fig.2.5) [Bolton, 1977]. Two conditions here are observed: (i) In case the electric circuit is not closed, the shift in Fermi level in the semi-conductor gives the open cell photovoltage, otherwise if closed via a counter electrode dipped into the same solution, the photovoltage is a driving force for electrolysis. Electric field for charge separation can also be obtained by the insertion of a p-n junction directly under the semi-conductor electrolyte interface. When the p-n junction is illuminated the photovoltage is directly available for electrolysis.



UNIVERSITY OF NAIRBE,  
CHIRANG LIBRARY

Fig.2.5 Energy relations in depletion layer for conduction band edge Fermi level in dark and on illumination.



## 2.8 Photovoltaic measurements

A Solar cell's performance is evaluated by determining the load characteristics of the device under illumination and obtaining the various photovoltaic performance characteristics. These performance characteristics include efficiency  $\eta$ , open circuit voltage  $V_{oc}$ , short circuit current  $I_{sc}$ , fill factor FF, maximum voltage  $V_m$ , maximum current  $I_m$  and maximum power  $P_m$ .

Solar cell measurements can be carried out either in natural sunlight or indoors using solar simulators. Recommended light sources for solar simulators used in terrestrial photovoltaic measurements include: (i) a dichroic filtered ELH-type tungsten lamp (ii) a short arc steady state xenon lamp and (iii) a long-arc pulsed xenon lamp. The spectral distribution of these sources match reasonably that of terrestrial sunlight.

Several types of equipment are used to obtain a solar cell I-V curve. These are: (i) fixed load resistors which allow only discrete points along the curve to be obtained. The maximum voltage drop across the cell on measuring the short circuit current should not exceed 20 mV. The open circuit voltage should be measured with a voltmeter of internal resistance of not lower than 20 K $\Omega$ /V. (ii) variable power supply: This device gives a continuous I-V curve. A sinusoidal signal is imposed on the device and the voltage and the current through the cell are fed to the X-Y axes of an X-Y recorder or oscilloscope with the current converted to a voltage signal by the use of a current - voltage converter. The advantage of this method is that it allows

the forward and the reverse biasing of the cell thus giving additional diagnostic information. (iii) electronic load: This is an automatic power supply specifically for solar cells. (iv) microprocessor based data acquisition system: This employs a power supply to obtain data.

In all these methods, great care should be taken in making electrical connections. Any wire resistance developed between the test device and the instrumentation causes power output losses and thus an inaccurate I-V curve.

The values  $V_{oc}$  and  $I_{sc}$  are read directly from the I-V curve obtained (see Fig. 2.6.)

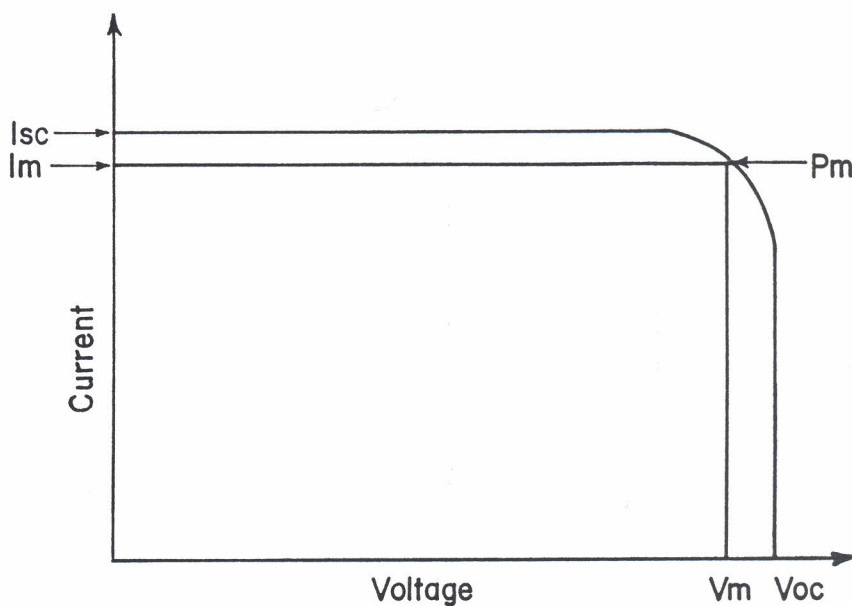


Fig. 2.6 Typical current-voltage curve for an ideal solar cell.

The maximum power point can be obtained by computing the IV product at various points along the curve and selecting the point where the product is a maximum. The voltage and current values at the maximum power point are the maximum voltage  $v_m$  and maximum current  $I_m$  values for the cell [Kastur and Suhit, 1983].

The maximum power,  $P_m$  and the fill factor, FF can be determined using the relation

$$P_m = V_m I_m \quad (2.19)$$

and

$$FF = V_m I_m / I_{sc} V_{oc} \quad (2.20)$$

This enables the efficiency  $\eta$  to be determined from

$$\eta = [ V_{oc} I_{sc} FF / P_{in} ] \times 100 \quad (2.21)$$

or

$$\eta = [ P_m / P_{in} ] \times 100 \quad (2.22)$$

where

$P_{in}$  is the illumination intensity incident on the cell.

### ***2.9 Spectral response investigation for solar cell***

This mainly involves the measurement of the wavelength dependence of the photocurrent. This is quite important both as a characterization technique and as an effective diagnostic and analytical tool. Any changes in the device configuration or material properties or electronic structure of the junction shows up in the spectral response curve.

## CHAPTER THREE

### 3 EXPERIMENTAL PROCEDURE

#### 3.1 Introduction

PEC solar cell development and fabrication procedures require the use of different materials and equipment, each of which has its appropriate stage of application. In this chapter, several processes involved in the development and fabrication of a metal sulfide PEC solar cell are reported where the apparatus and techniques used are also presented.

##### 3.1.1 Spray pyrolysis

The spray pyrolysis is a chemical deposition technique that involves spraying a solution, usually aqueous, containing soluble salts of the constituent atoms of the desired compound onto a substrate maintained at elevated temperatures.

Spray pyrolysis involves a thermally stimulated reaction between clusters of liquid/vapour atoms of different chemical species. The sprayed droplet reaching the hot substrate surface undergoes endothermic pyrolytic decomposition and this forms a single crystallite or a cluster of the product. The by-products which are mainly volatile together with the excess solvent escape in the vapour phase.

The thermal energy for the decomposition of the constituent species comes from the substrate. This is followed by sintering and recrystallization of the clusters of crystallites thus giving rise

to a coherent film. This technique, besides being a technique suitable for large scale film production gives the researcher an opportunity to optimize parameters and variables like temperature of the substrate and deposition flow rate.

The spray pyrolysis setup (as shown in Fig. 3.1) comprised a sprayer made of hard glass. The sprayer had two inlets. One inlet allowed in pressurized carrier gas (nitrogen) while the other allowed the inflow of the solution to be sprayed. The solution and the carrier gas had a common outlet, and the solution emanated as a cone due to the pressurized gas. The pressurized solution fell on a substrate at elevated temperatures forming a film. The substrate temperature was maintained constant with the help of an electric heater whose heat input was controlled by the use of a variac. A 2100A Flukes digital thermometer was used for monitoring the substrate temperature.

The solution was sprayed for a few seconds (between 4-7 s) then stopped to give time for the temperature of the substrate to rise back to the optimized value. The process was continued until the required coating was obtained. The intermittent spraying helped prevent the cracking of the substrate owing to rapid cooling. To obtain a uniform film, the sprayer was moved to and fro above the substrate in a plane parallel to the substrate. The substrate was turned through  $180^\circ$  after approximately half the solution was sprayed. This helped in reducing the likelihood of one end of the substrate being sprayed on more than the other. It was not likely for multilayers to form because

there was very little time difference (1-3 secs) between one phase of spray and the next. This was made possible by not letting the substrate temperature to fall far below the optimized value (range was 1-2 ° C).

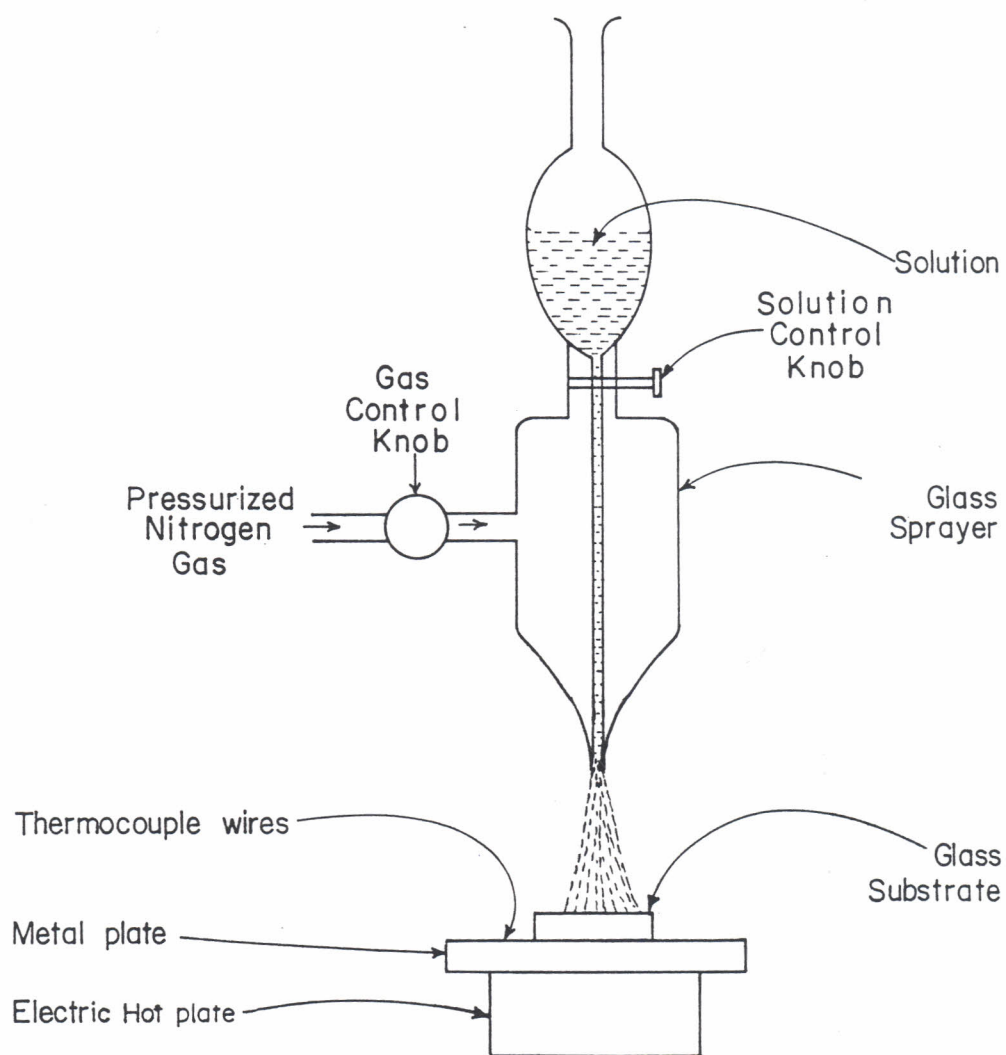


Fig.3.1 Schematic diagram of the spray pyrolysis setup.

### **3.2 Preparation of samples and solar cell studies**

The methodology involved in the present investigation included six basic steps.

- i) optimization of spray parameters
- ii) preparation of iron disulfide
- iii) photoelectrode preparation
- iv) iron disulfide characterization
- v) investigation on optical transmittance of photoelectrode
- vi) PEC solar cell studies.

The method used in the preparation of the iron disulfide was the spray pyrolysis method followed by sulfurization.

#### **3.2.1 Optimization of parameters**

The spray rate, substrate spray temperature, height of spray above the substrate, and the solutions to be sprayed were optimized by visually observing the nature of film formed. A series of experiments were conducted by keeping some parameters constant and varying a parameter at a time until all parameters were optimized. A coherent, uniform film without visible pinholes was expected at the optimized parameters. By observing the film against light, thinner sections could be seen if it was not of uniform thickness. The annealing rates in sulfur were optimized by (i) determining the heating and cooling rates that resulted in total conversion of the iron oxide to iron disulfide. This was determined by visual observation of the film underside. The underside colour of the film was expected to be gold-like when conversion was complete. (ii) determining the rates that did not cause



peeling off of the iron oxide film.

The cell's electrolyte was optimized with respect to its optical transmittance and resistance.

Low resistance and high transmittance was expected.

### **3.2.2 Preparation of iron disulfide**

Four basic steps were followed in the preparation of iron disulfide (iron pyrite):

- i) cleaning of the substrate
- ii) deposition of iron oxide by spray pyrolysis
- iii) conversion of iron oxide into iron disulfide
- iv) removal of sulfur from prepared film.

#### **(i) Cleaning of Substrates**

The substrates used were glass slides measuring 3.75 by 2.5 by 0.1 cm. Prior to deposition, the glass substrates were cleaned by hand using cotton-wool and soap. This removed the grease detectable by the human eye. A lens cleaning soft tissue paper was slowly run over the substrates to remove most of the soap and dirt. The substrates were then dipped into acetone several times to remove any stubborn stains. Finally, they were dipped into isopropyl alcohol and thereafter in distilled water. The cleaned glass substrates were kept in an oven at about 60 °C ready to be coated on.

## **(ii) Deposition of iron oxide**

Iron oxide was grown on a clean glass substrate at elevated temperatures (370.0 °C) by spray pyrolysis by spraying iron (III) chloride solution. The deposition was done in air and thus the most likely oxide was hematite( $\text{Fe}_2\text{O}_3$ ).

## **(iii) Conversion of iron oxide into iron disulfide**

Conversion of iron oxide into iron pyrite was achieved by annealing the oxide in sulfur vapour; a process called sulfurization [See fig. 3.2]. The oxide-coated substrate was laid on top of a 'U' shaped metal plate which was in turn placed on top of a flat metal plate placed on top of an electric heater. The flat metal plate was used both as a flat surface on which the 'U' shaped metal plate with the sample rested and as an indirect contact between the electric heater and the sample. The 'U' shaped metal plate prevented the flow of melted sulfur onto the substrate. A glass container open at its base and with a tightly fitting lid (at the top) with a small exhaust hole (near the top) was inverted over over the 'U' metal plate and sample. About 2.4 - 3.0 g of powdered sulfur was evenly spread on the flat metal plate area enclosed by the inverted glass container but outside the 'U' metal plate. A bigger glass container was used to enclose the system. The temperature was slowly raised to 350.0 °C then slowly reduced down to below 80.0 °C.

A likely equation for the reaction was [Smestad et al and Kautek, 1990]:



$$\Delta G = -42.8 \text{ KCal/mol}$$

#### (iv) Removal of sulfur from iron disulfide film

The prepared samples were dipped several times in carbon disulfide to dissolve away any sulfur on the film surface. The samples were then rinsed with distilled water.

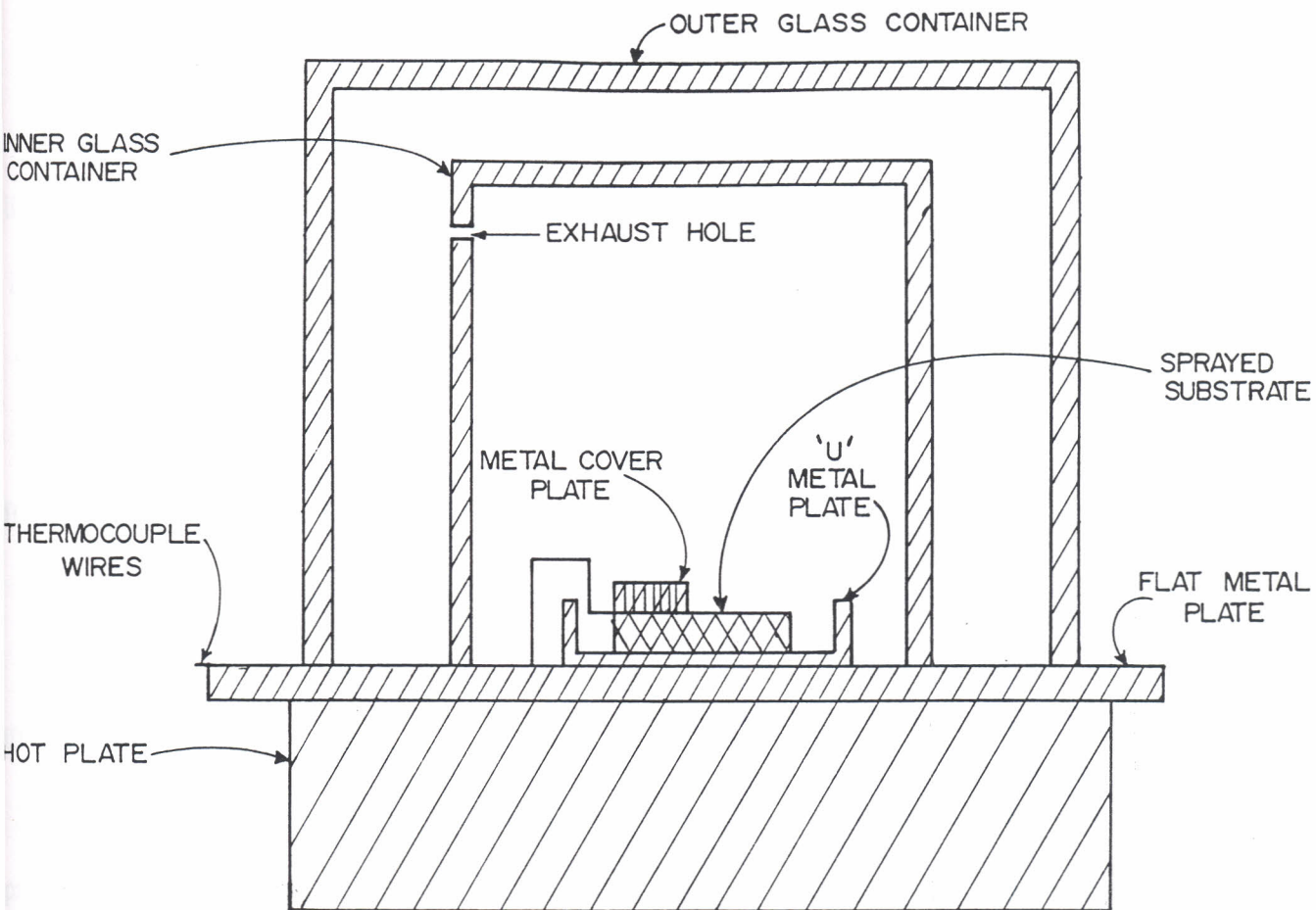


Fig.3.2 Schematic experimental setup of the sample annealing

#### **(v) Determination of film type**

Thermoelectric method was used to test whether the films grown were n or p type.

### **3.2.3 Photoanode preparation**

The preparation of the photoelectrode included five sequential steps. These were:

- i) cleaning of substrate
- ii) deposition of back contact
- iii) deposition of iron oxide
- iv) conversion of iron oxide into iron disulfide
- v) removal of sulfur from the photoelectrode.

#### **(i) Cleaning of substrate**

The glass substrates were cleaned as described in section 3.2.2(i).

#### **(ii) Deposition of back contact**

Tin oxide was used as a back contact for the photoelectrode. It was deposited on the substrate by spray pyrolysis as described in section 3.1.1. Prior to obtaining a good and low resistance back contact, optimization had to be done with respect to deposition rate, height of spray nozzle above the substrate, substrate temperature and the ratios of mixing of the solutions to be sprayed.

The deposition rate was obtained by determining the time it took a given volume of solution to be sprayed. A series of trial experiments were conducted to determine the best spray rate at different heights above the substrate. The best substrate temperature and ratio of mixing of the solutions were also determined.

A solution of anhydrous tin (IV) chloride also known as stannous chloride and isopropyl alcohol were mixed and ammonium fluoride was added to this solution. The solution was sprayed on a glass substrate at elevated temperatures (420.0 °C). The molarities, and temperature were varied in an attempt to optimize the oxide formed.

### **(iii) Deposition of iron oxide**

The method for the deposition of iron oxide was as described in section 3.2.2(ii). However, having deposited the back contact on the substrate, the iron oxide was grown on only a portion (about half) of the section with the back contact coating. This was achieved by covering the rest of the back contact film with a metal plate.

### **iv) Annealing in sulfur vapour**

The conversion process was done as in section 3.2.2(iii) the only difference being that the portion covered (see section 3.2.3(iii)) still remained covered during the annealing process.

#### **(v) Removal of sulfur from the photoanode**

Carbon disulfide and distilled water were used as described in section 3.2.2(iv) to remove sulfur from the photoelectrode. Two photoelectrodes designated A and B were prepared. Photoelectrode B was annealed in vacuum at a pressure of about  $8-9 \times 10^{-5}$  Torr for 3.5 hrs at a temperature of about  $140.0^\circ\text{C}$ , etched in hydrogen fluoride, ethanoic acid and nitric acid in the ratio 1:1:2 after preparation. Photoelectrode A was neither vacuum-annealed nor etched.

### **3.2.4 Iron disulfide characterization**

#### **(i) X-ray diffraction**

X-ray diffraction pattern was taken in the  $2\theta$  geometry with a diffractometer using a  $\text{Cu K}\alpha$ - $105414 \text{ \AA}$  anode.

#### **(ii) Optical studies**

An SPS 150 UV/Visible Spectrophotometer was used in this study. The ratio recording technique was used. In this method, the optical transmittance of a thicker pyrite film relative to a thinner one was measured. The transmittance ratio  $T_{1/2}$  is given by

$$T_{1/2} = \exp(-\alpha\Delta t) \quad (2.25)$$

This is equivalent to measuring the transmittance of a film of thickness  $\Delta t$ . With the transmittance known and the thickness determined, then  $\alpha$  the absorption coefficient was determined.

The transmittance of the photoelectrode was also measured using a blank substrate as reference.

### (iii) Determination of film thickness

This was measured by the weighing method. The substrate was first weighed with the back contact coating. It was reweighed after the iron pyrite film was formed and the difference in mass ( $\Delta m$ ), calculated. The difference was the mass, ( $\Delta m$ ) of the pyrite film. Knowing the density ( $\rho$ ) of iron pyrite ( $5.02 \text{ g/cm}^3$ ), the film thickness was calculated from [Lona, 1997]

$$\Delta t = \frac{\Delta m}{\rho A} \quad (2.26)$$

where

A = coated area

UNIVERSITY OF NAIROBI  
CHIROMO LIBRARY

### 3.2.5 Photoelectrochemical solar cell studies

PEC solar cell studies begun with the optimization of the electrolyte and determination of the optical transmittance of the cell container.



### **(i) Optimization of electrolyte**

The electrolyte used was an aqueous solution of potassium iodide and iodine. A series of trial experiments were conducted to optimize the electrolyte with respect to current, voltage, resistance and optical transmittance. The optical transmittance as a function of wavelength is as shown in Fig. 4.4.

The transmittance of the cell container was measured using an SPS 150 UV/Visible Spectrophotometer.

### **(ii) Cell setup**

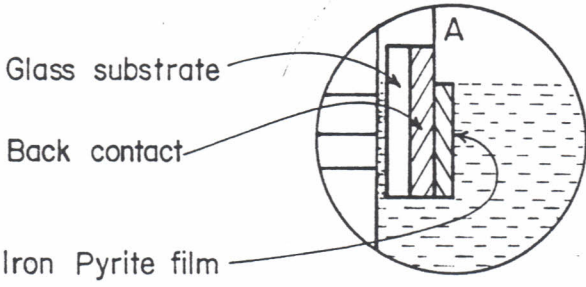
The cell setup is shown in Fig.3.3. A 17 V, 150 W Quartz Halogen dichroic mirror lamp (Phillips) having spectrum approximating that of the sun was used to irradiate the photoelectrode. The cell was kept in a closed chamber with a window through which light could be allowed to shine on to the photoelectrode. The cell container made from perspex had internal dimensions of about 4.2 by 3.8 by 3.1 cm and a thickness of 0.2 cm. The active area of the photoelectrode was calculated from the film width and the area of the film in electrolyte. The corresponding photovoltages and currents were noted down.

### **(iii) Illumination intensity measurements**

The illumination intensity measurements were carried out using a Kipp and Zonen CM5/6 Solarimeter with a thermopile resistance of  $10.1 \Omega$ . The Solarimeter was illuminated with the same

intensity as the cell and the corresponding value of the illumination intensity in millivolts read from a 1905a Intelligent digital Multimeter connected to the Solarimeter. By the use of the conversion relation  $1000 \text{ W/m}^2 = 11.8 \text{ mV}$  for the particular solarimeter, the illumination intensity was converted into  $\text{W/cm}^2$ .

SIDE VIEW OF ENLARGED PHOTOANODE



- A — Photoanode
- B — Counter electrode
- C — Perspex cell container

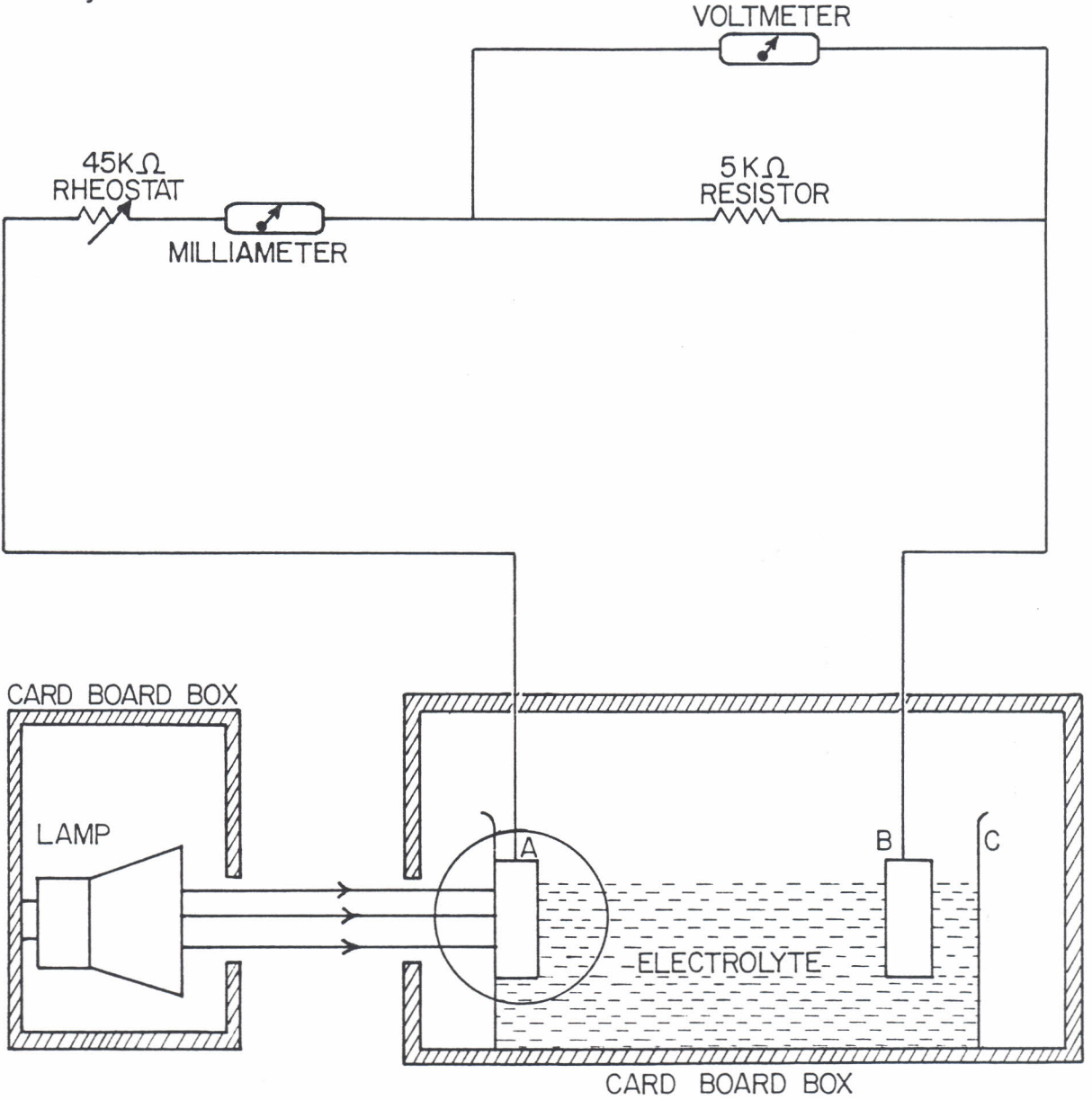
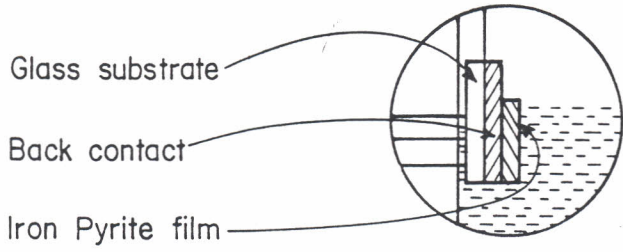


Fig. 3.3 PEC solar cell setup.

#### **(iv) Spectral response investigation**

Monochromatic photons of known wavelengths were allowed to impinge upon the photoelectrode surface and the corresponding short circuit current noted to determine the spectral characteristics of the cell under study. In this work, a Phillips 150 W Quartz Halogen dichroic lamp was used as the source of the radiation. Collimated light from this source was imposed upon the cell through colour filters which allowed a narrow bandwidth centered around a known wavelength to pass through (Fig. 3.4). The intensity was controlled by reducing or increasing the supply voltage.

SIDE VIEW OF ENLARGED PHOTOANODE



- A — Photoanode
- B — Counter electrode
- C — Perspex cell container

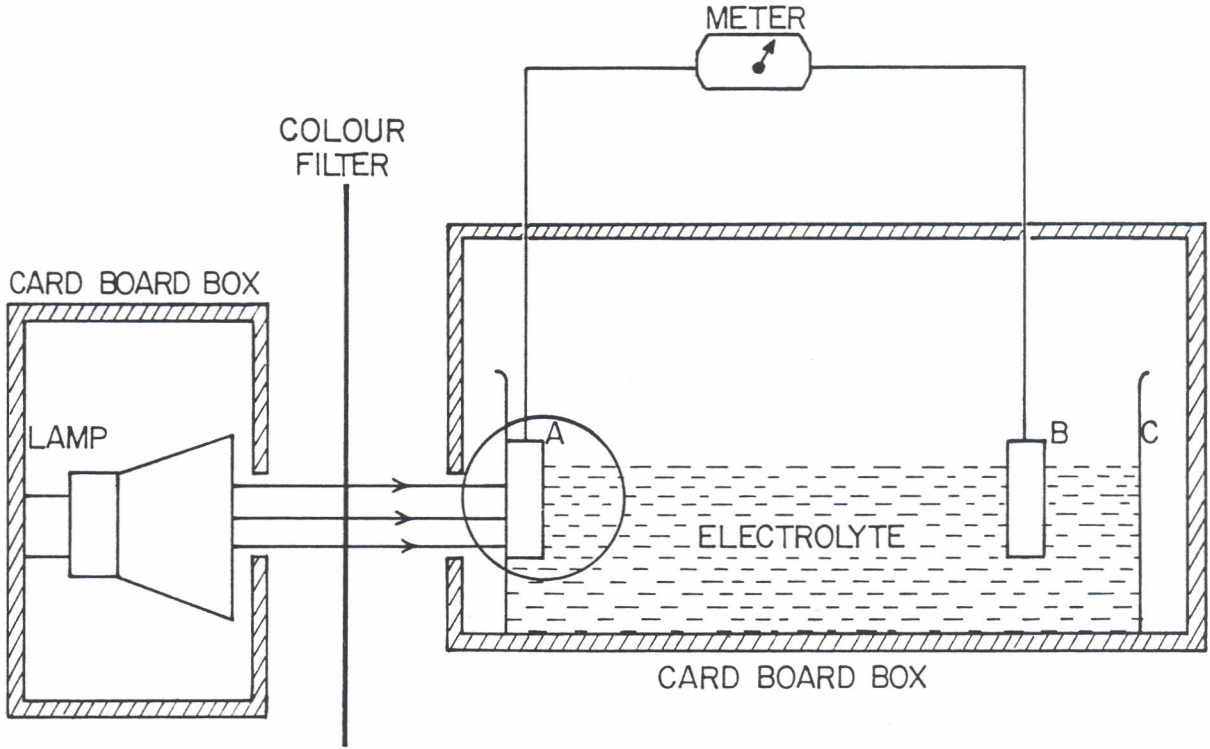


Fig. 3.4 Spectral response measurements for PEC solar cell.

## CHAPTER FOUR

### 4 RESULTS AND DISCUSSION

#### 4.1 Optimization of parameters

The optimized parameters and the quantities used in the spray process are presented. The best spray rate was determined as 14.0 ml/min. A spray height of 30-35 cm above the substrate was found to be appropriate at the above spray rate.

The optimized masses and volumes of chemicals/solutions used in the preparation of back contact were found to vary. It was established that a solution made of 5.0 cm<sup>3</sup> tin (IV) chloride, 5.0 cm<sup>3</sup> isopropyl alcohol and 0.0854 g ammonium fluoride when sprayed produced the best film. The resulting films were transparent and of very good adhesion [Kaustur and Suhit, 1983]. They had a violet/purple colour when viewed against light and had a sheet resistance of 22.0  $\Omega/\square$ . Sheet resistance is the resistance of a film when its length is equal to its width.

The molarity of the iron (III) chloride sprayed was 0.1. The established best substrate spray temperature was 370.0 °C.

Optimization was also done with regard to annealing of iron oxide film in sulfur vapour. The best annealing rates were 4-5 °C/min and 1-2 °C/min for heating up and cooling down respectively. The highest temperature reached during the heating up process was 350.0 °C while cooling was done down to below 80.0 °C. It was established that higher heating or cooling rates resulted in the peeling off of the film. The resistance of the optimized film was measured to be about 6.0 K $\Omega$ .

## 4.2 Characterization of iron disulfide film

XRD diffraction measurements carried out using a Cu K $\alpha$ -1.5414 Å radiation gave the pattern shown in Fig.4.0. Comparison of the obtained pattern with data in diffraction data book [Mines and Geology, Industrial area, Kenya] and results obtained by other authors [Smestad and Silva, Tributsch et al, 1988; Ferrer and Sa'nchez, 1991; Hopfner et al, 1995; Smestad et al and Kautek, 1989; Ennaoui et al, 1992] confirmed the material to be iron pyrite.

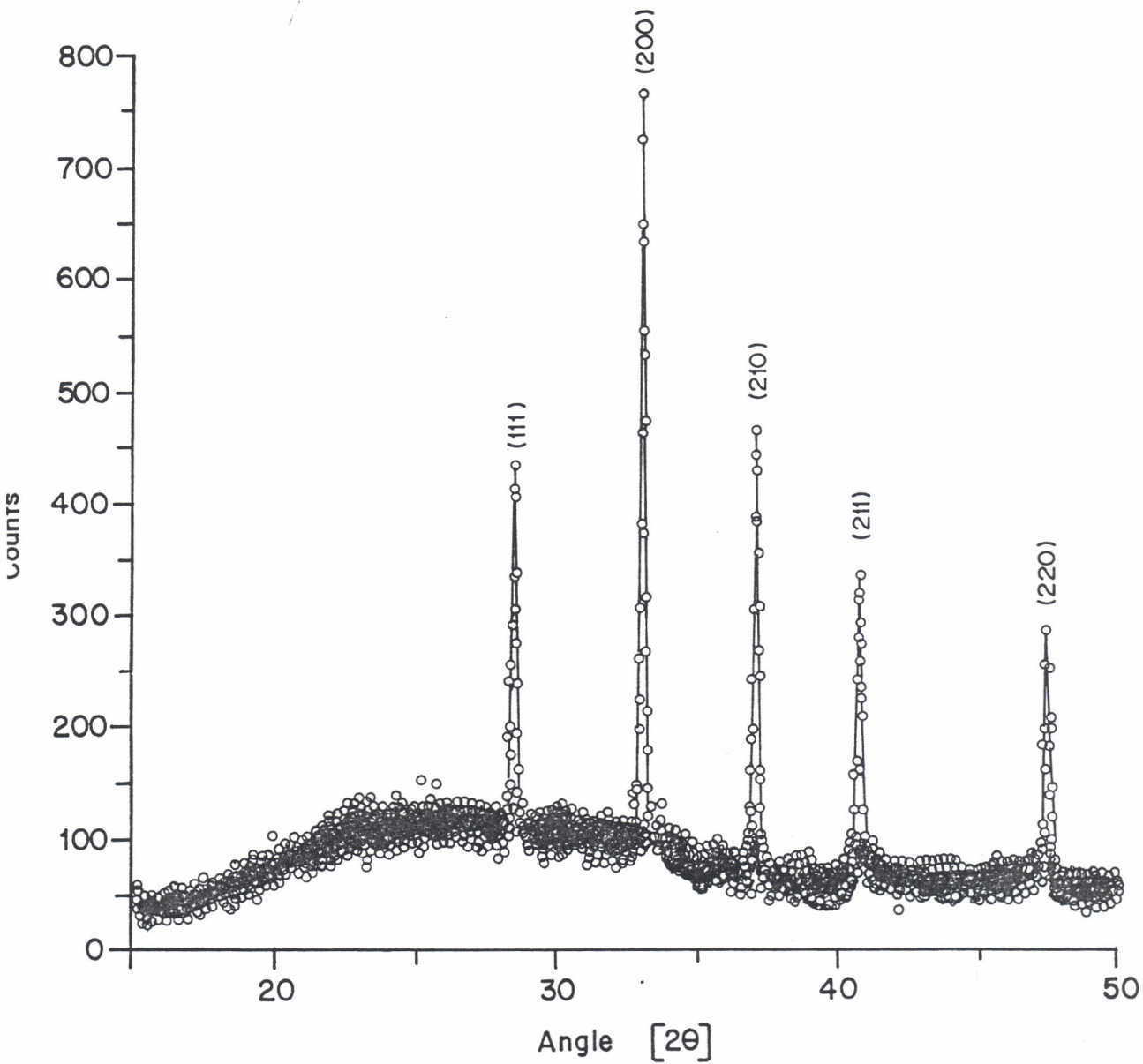


Fig. 4.0 XRD Pattern for films prepared by spray pyrolysis followed by sulfurization.



Tests carried out using the thermoelectric effect did not indicate the material (iron disulfide) to be distinctly n or p type. A possible explanation for non-distinctness in the type of film is the possibility of ion compensation. Iron vacancies must exist for a p type material while sulfur vacancies must be there for a n type material. When these vacancies are almost in equal numbers, there is compensation and the material may not show a distinct type [Schieck, 1990]. However, when used in the PEC solar cell a current must flow thus indicating the type of the material. The current direction in our solar cell indicated that the films were n type.

The mass of the iron pyrite on the substrate was measured to be  $3.51 \times 10^{-3}$  g. The length and width of the iron pyrite on the substrate was measured as 2.0 cm and 2.5 cm respectively giving the area, A, as  $5.0 \text{ cm}^2$ . Given the density of iron pyrite to be  $5.02 \text{ g/cm}^3$ , the thickness of the iron pyrite film was found to be  $1.4 \text{ }\mu\text{m}$ .

Figure 4.1 shows how the absorption coefficient of iron disulfide varies with photon energy. The data is tabulated in Table 4.1.

Table 4.1 Optical transmittance for iron pyrite film.

Wave length $\lambda$ (nm)	600	700	800	892	918	946	961	984
Photo energy (ev)	2.06	1.77	1.55	1.39	1.35	1.31	1.29	1.26
Transm (%) T	0	0	.01	.03	.62	1.04	2.39	3.81
Absorb. Coeff. $\alpha \times 10^4/cm$	-	-	6.53	5.75	3.61	3.24	2.65	2.32

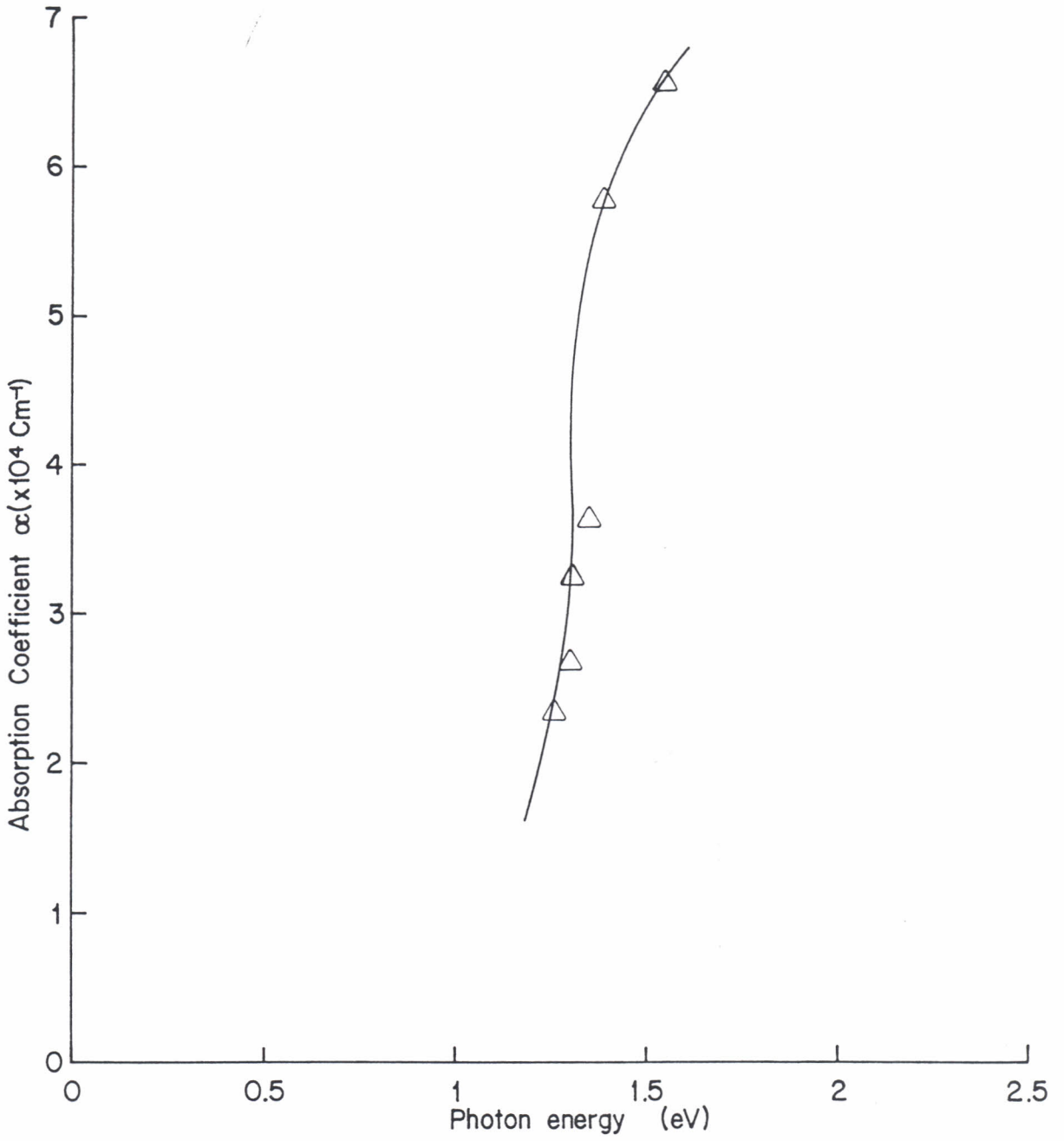


Fig.4.1 Absorption coefficient for Iron Pyrite versus photon energy.

An absorption band edge was obtained around 1.0 eV. The same value (1.0 eV) was obtained by Hopfenner and others [Hopfenner et al, 1995]. Other researchers [Ennaoui et al, 1986; Ennaoui et al, 1992; Giersig et al, 1992; Schieck et al, 1990] have obtained a value of 0.95 eV which again is rather close to our value. The absorption coefficient ( $\alpha$ ) for iron disulfide was found to be in the range of  $3 \times 10^4 \text{ cm}^{-1}$  at 1.3 eV. This shows and confirms its future potential as a solar cell material. A number of researchers [Hopfenner et al, 1995; Smestad et al, 1989; Schieck et al, 1990] have obtained values of  $\alpha > 10^5 \text{ cm}^{-1}$  at values of energy  $< 1$  eV. However, it should be borne in mind that these results were given by n type crystals prepared by either chemical vapour deposition (CVD) or metal organic chemical vapour deposition (MOCVD) method. Nevertheless, the value of  $\alpha$  obtained in our work still compares rather well with that obtained by the above researchers. One of the reasons for the low value of absorption coefficient obtained in our work could be attributed to the possible existence of small micro pinholes on the iron pyrite film produced during fabrication. The pinholes have the effect of allowing radiation to pass through thus reducing the absorption [Ennaoui et al and Giersig; Vogel and Weller, 1992].

### **4.3 Photoanode transmittance studies**

Transmittance studies of photoanode prepared by spray pyrolysis and sulfurization were carried out.

Photoanode's optical transmittance before and after use in the cell are given in Tables 4.2 and 4.3 respectively and their corresponding graphical representations in Figure 4.2.

Table 4.2 Optical transmittance for a photoanode before use in the cell.

Wave Length $\lambda$ (nm)	400	600	800	820	840	860	880	890	900
Transm (%)	0	0	0.10	0.04	0.95	1.56	3.65	5.78	7.85

Table 4.3 Optical transmittance for a photoanode after use in the cell.

Wave Length $\lambda$ (nm)	400	600	650	750	820	850	875	900
Transm (%)	0	0	0.02	0.09	1.10	1.56	4.21	8.02

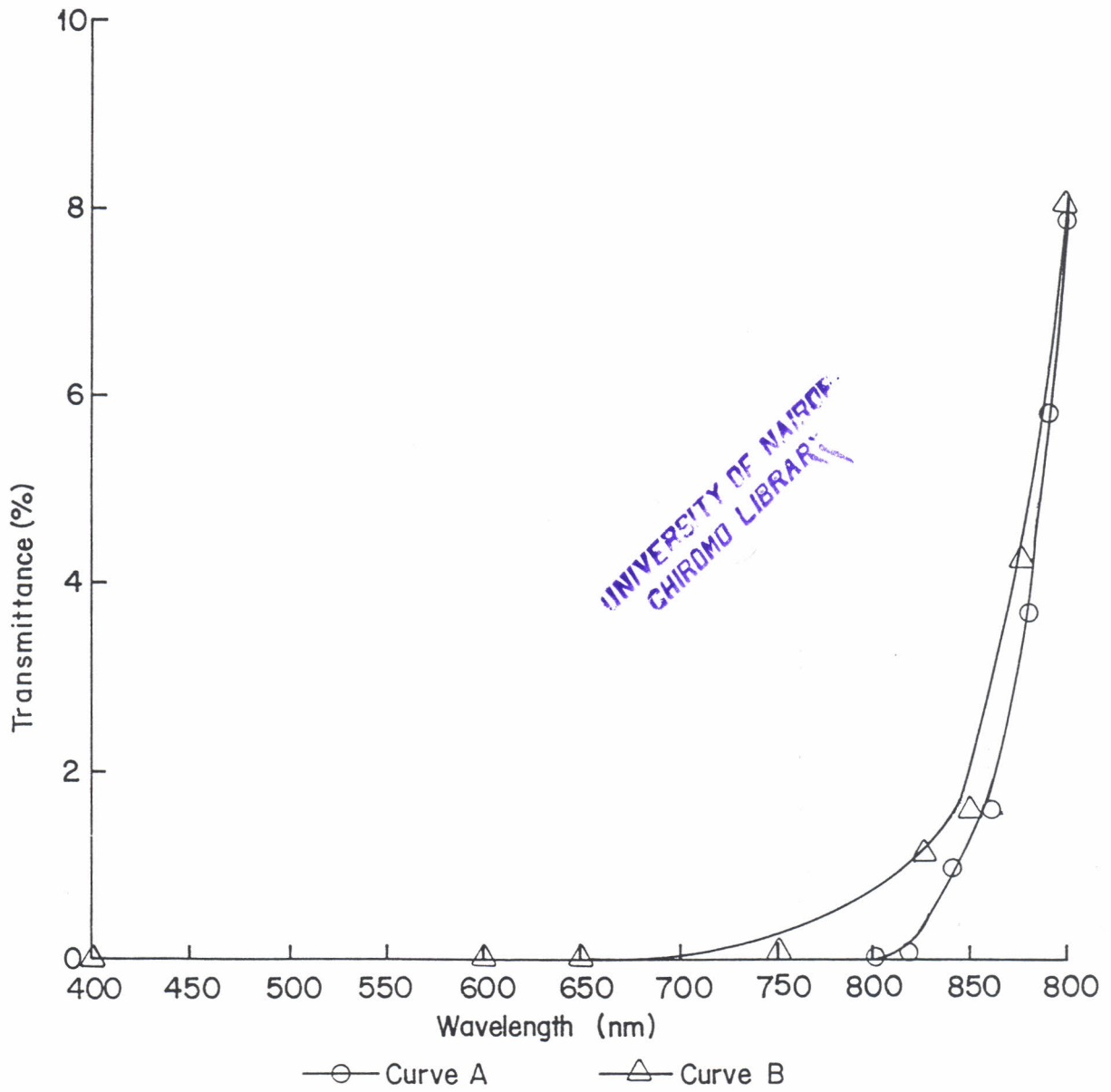


Fig.4.2 : Optical transmittance versus wavelength for a photoanode before (curve A) and after (curve B) use in solar cell .

The percentage optical transmittance of a photoanode used in our solar cell was measured as a function of wavelength of the radiation before and after use. It can be seen from the foregoing results (Fig.4.2) that the photoanode is opaque to radiation of wavelengths from 400-750 nm. All the radiation falling on the photoanode in this range was absorbed. Comparing the optical transmittances of the photoanode before and after use in our cell, it is clearly noted that optical transmittance for the used photoanode starts at 650 nm wavelength. A plausible explanation to this observation lie in the possible photocorrosion of our iron pyrite film. This is a major problem in these types of solar cells [Ennaoui et al, 1986] and it is likely that the photocorrosion of the photoanode causes the pyrite film to become thinner or even may lead to the creation or enlargement of pinholes. Creation or enlargement of pinholes allows more radiation to pass through.

#### **4.4 Electrolyte studies**

Table 4.4 gives the optical transmittance values of the electrolyte used in our study with a graphical representation in Fig. 4.3.

An electrolyte concentration of 3.0 M potassium iodide (KI) and 0.01 M iodine(I<sub>2</sub>) was found to be suitable for our cell. This electrolyte had a percentage optical transmittance of between 47.5 - 95.2 for the wavelengths 600 - 800 nm (see Fig. 4.3). On illumination, 9.90 mV and 0.012 mA were obtained as the open circuit voltage and short circuit current respectively.

The conductance of the electrolyte was found to be about  $0.2 (\Omega M)^{-1}$ .

Table 4.4 Optical transmittance(%) values of electrolyte in the visible wavelength range.

Wave Length $\lambda$ (nm)	480	500	530	580	600	750	800	900
Transm (%)	0	2.9	11.0	30.1	52.5	94.2	95.2	99.5

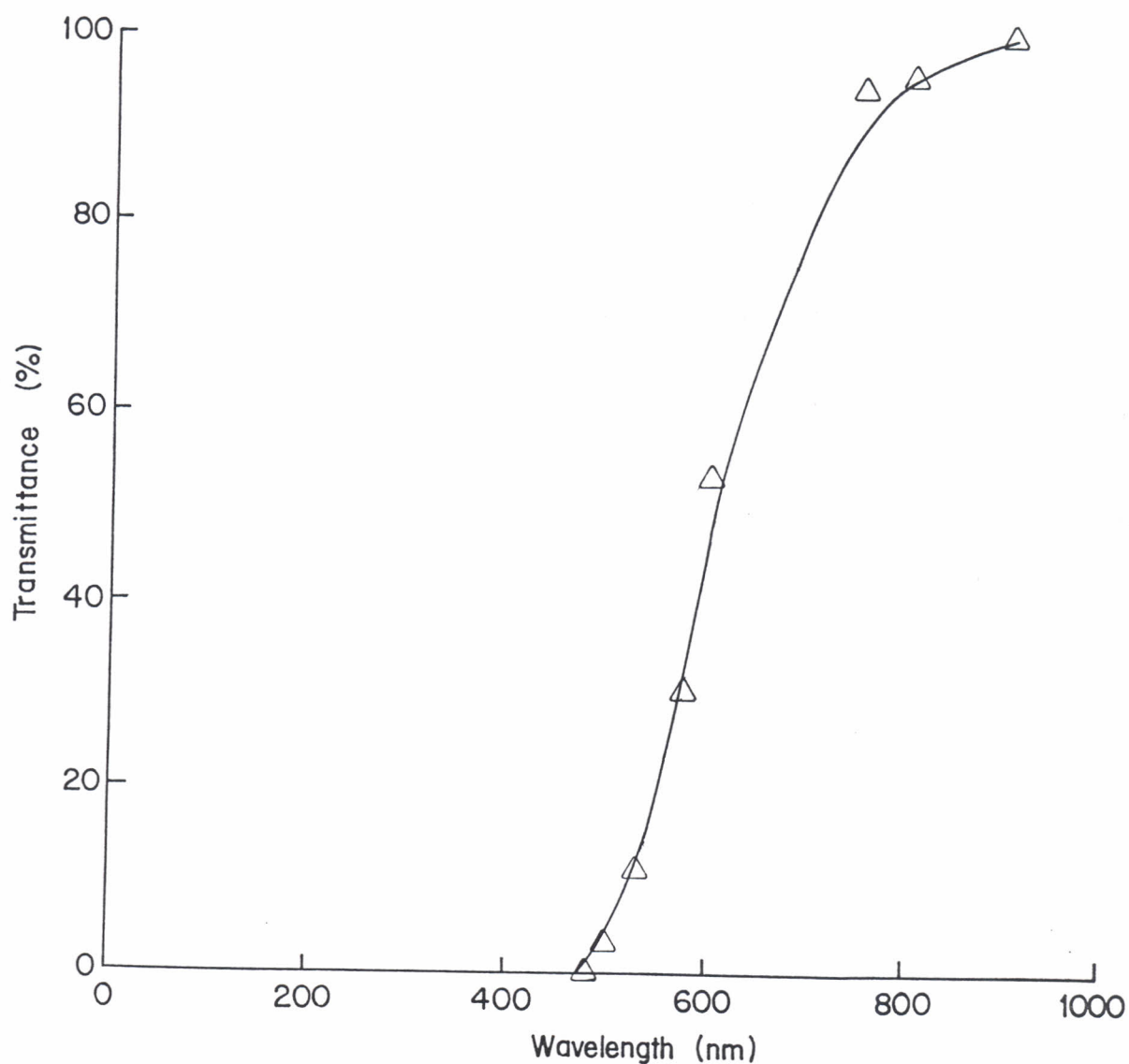


Fig. 4.3 Optical transmittance of electrolyte versus wavelength.



### 4.5 Transmittance of cell container

Presented in Fig.4.4 is the cell-container percentage optical transmittance versus wavelength of incident radiation characteristic, plotted from Table 4.5.

Table 4.5 Optical transmittance (%) of cell container in the visible wavelength range.

Wave Length $\lambda(\text{nm})$	400	450	500	600	650	700	750	800	850
Transm (%)	86.7	87.1	88.1	90.1	91.2	92.0	92.3	92.4	92.5

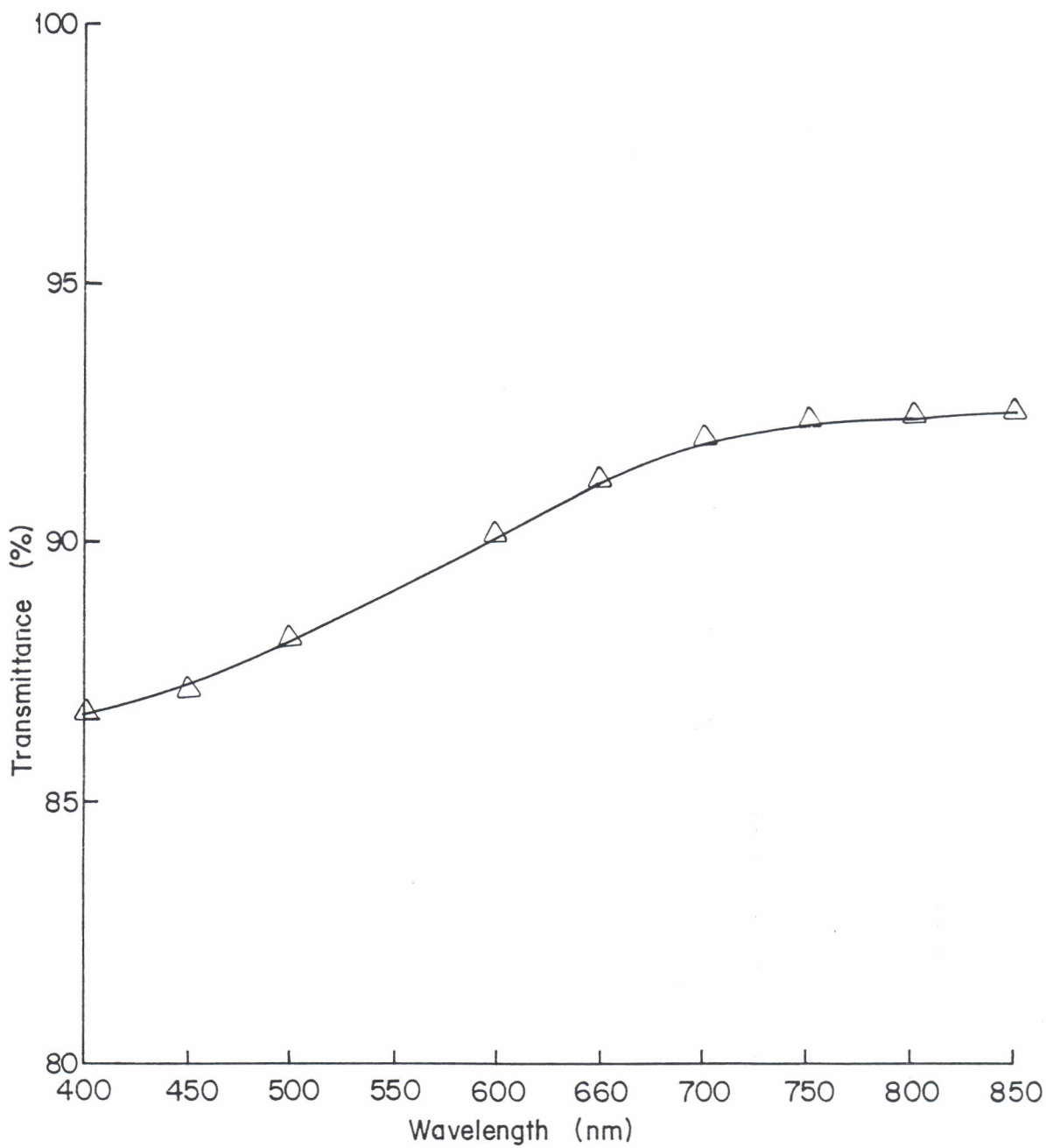


Fig.4.4 Optical transmittance of cell container versus wavelength.

### 4.6 Photoelectrochemical solar cell

Studies of the PEC solar cell output were carried out using two photoanodes; photoanode A and B. Both photoanodes were prepared as described in chapter 3, however, photoanode B was vacuum-annealed as in section 3.2.3(v) while photoanode A was neither vacuum-annealed nor etched. The active area of the photoanodes was 1.0 cm<sup>2</sup> and the illumination intensity was 546.3 mW/cm<sup>2</sup> (these were the values used in our cell unless otherwise stated).

Table 4.6 shows the data collected with the optimized electrolyte and photoanode, with the corresponding graph of current density against photovoltage (on illumination) appearing in Fig. 4.5.

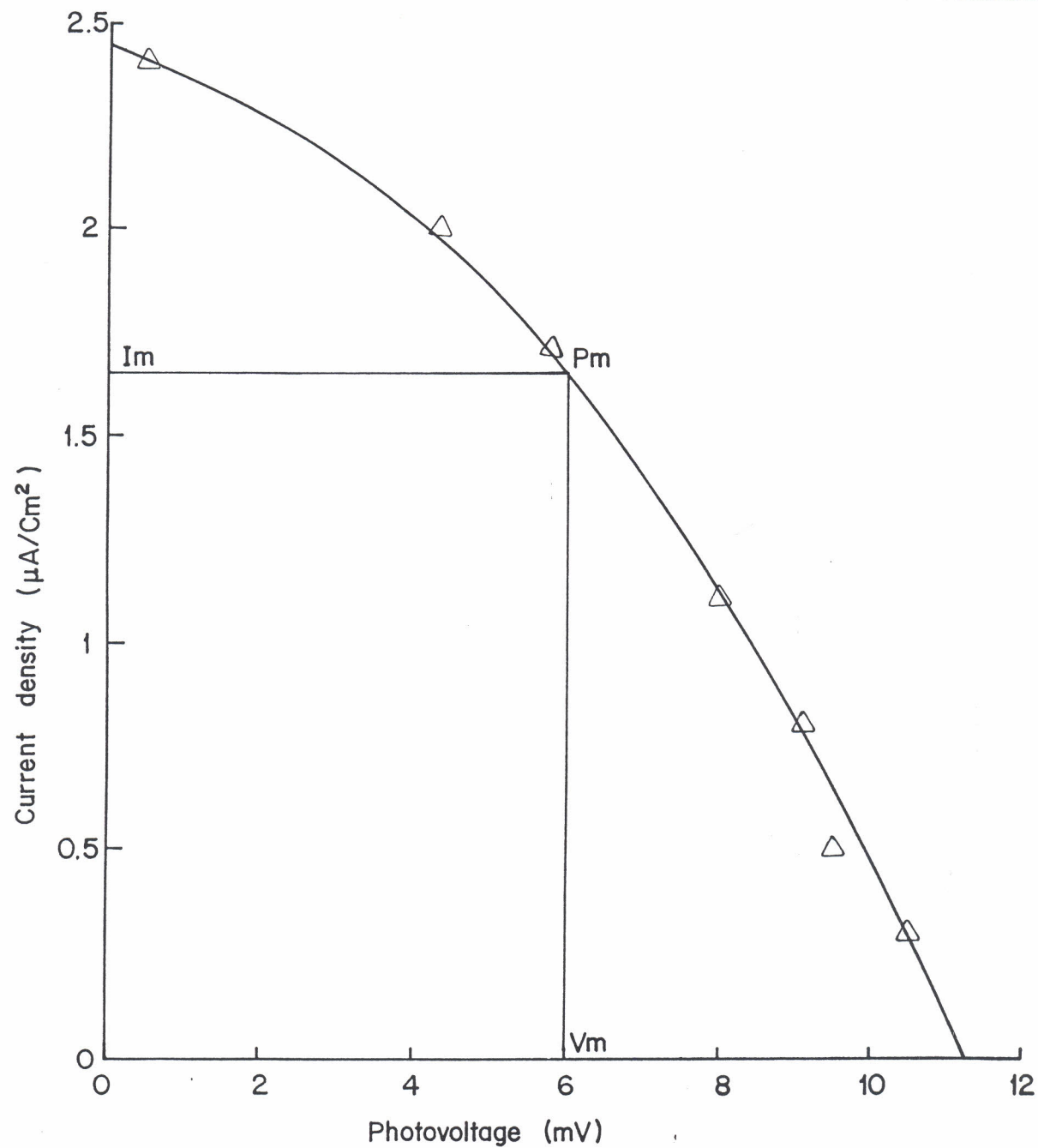
Table: 4.6. Photocurrent and photovoltage values on

illumination for photoanode A.

Illumination intensity = 546.3 mW/cm<sup>2</sup>.

CURRENT ( $\mu\text{A}$ ) (-VE)	2.4	2.0	1.7	1.1	0.8	0.5	0.3
CURRENT DENSITY ( $\mu\text{A}/\text{cm}^2$ ) (-VE)	2.4	2.0	1.7	1.1	0.8	0.5	0.3
PHOTO- VOLTAGE (mV)	0.5	4.3	5.8	8.0	9.1	9.5	10.5

The electrical output values of iron pyrite PEC solar cell with photoanode A are given in Table 4.7, on the other hand, Table 4.8 contains values of the electrical output of the solar cell with photoanode B.



75  
Fig. 4.5. I-V Characteristic curve for a photoelectrochemical solar cell with photoanode A on illumination.

Table. 4.7. Electrical output values of photoanode A for PEC

solar cell fabricated in our laboratory.

PHOTO-VOLTAGE AT MAX. POWER POINT (V <sub>mpp</sub> )	PHOTO-VOLTAGE AT MAX. POWER POINT (I <sub>mpp</sub> )	SHORT CIRCUIT CURRENT (I <sub>sc</sub> )	OPEN CIRCUIT VOLTAGE (V <sub>oc</sub> )	FILL FACTOR (FF)	EFFI-CIENCY (η)
6.0 mV	1.67 μA/cm <sup>2</sup>	2.42 μA/cm <sup>2</sup>	11.1 mV	0.373	1.83 10 <sup>-6</sup> %

Table 4.8 Photocurrent and photovoltage values and on

illumination for photoanode B.

CURRENT (μA) (-VE)	40.0	37.5	34.5	31.5	21.0	0.5
CURRENT DENSITY (μA/cm <sup>2</sup> ) (-VE)	40.0	37.5	34.5	31.5	21.0	0.5
PHOTOVOLTAGE (mV)	0.27	15.25	32.57	48.27	60.50	64.46

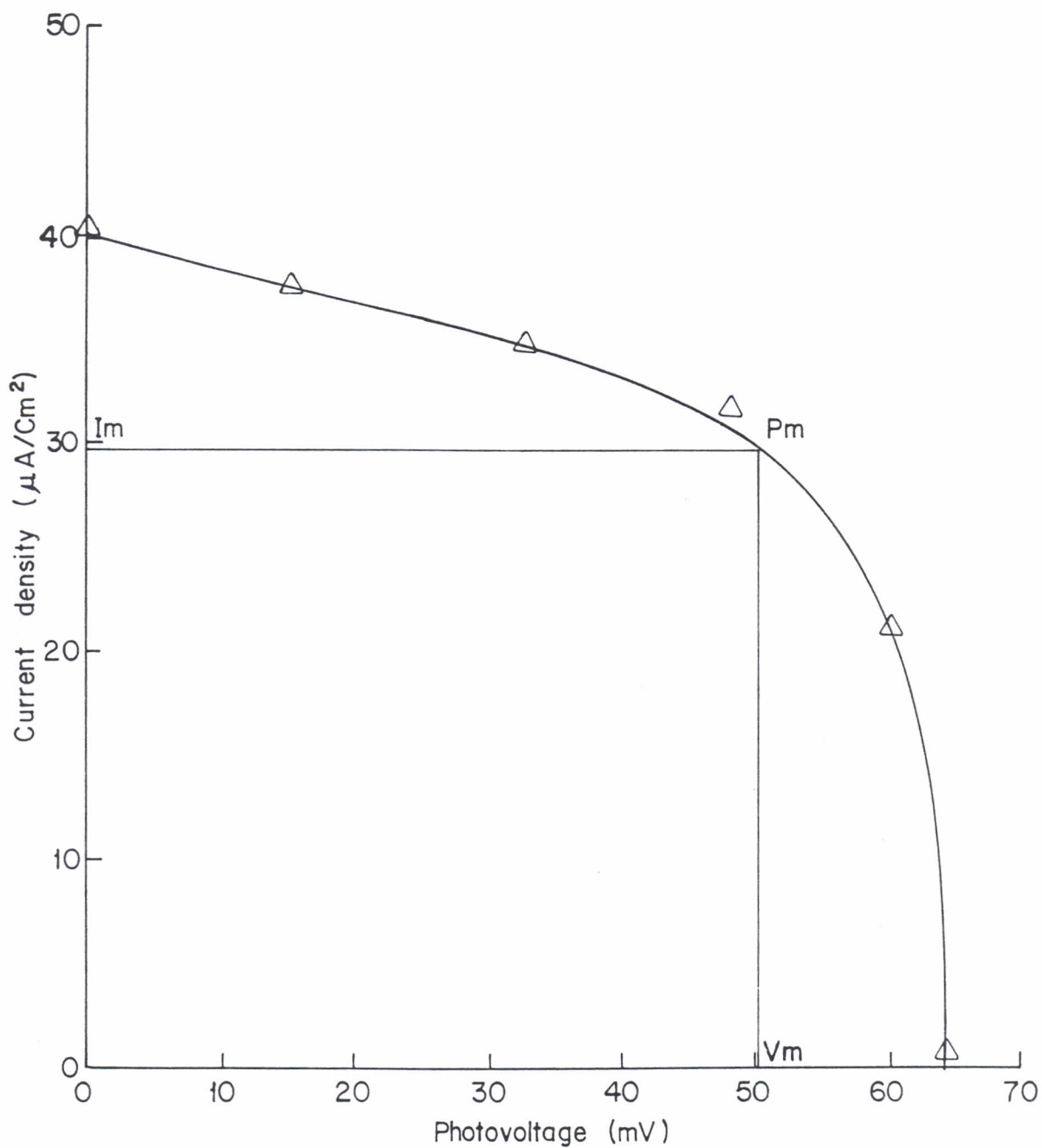


Fig. 4.6 : I - V Characteristic curve for a photoelectrochemical solar cell with photoanode B on illumination .

Table 4.9 Electrical output values for photoanode B obtained from PEC solar cell.

PHOTO-VOLTAGE AT MAX. POWER POINT (V <sub>mpp</sub> )	PHOTO-VOLTAGE AT MAX. POWER POINT (I <sub>mpp</sub> )	SHORT CIRCUIT CURRENT (I <sub>sc</sub> )	OPEN CIRCUIT VOLTAGE (V <sub>oc</sub> )	FILL FACTOR (FF)	EFFICIENCY (η)
49.45 mV	30.0 μA/cm <sup>2</sup>	40 μA/cm <sup>2</sup>	64.46 mV	0.575	2.71X 10 <sup>-4%</sup>

The foregoing results indicate a photocurrent density of 1.67 μA/cm<sup>2</sup> and a photovoltage of 6.0 mV for photoanode A at maximum power points, whereas photoanode B had 30.0 μA/cm<sup>2</sup> as photocurrent density and 49.45 mV as photovoltage at maximum power point respectively. The values are an improvement on the 1.0 mV and 1.0 μA/cm<sup>2</sup> obtained by Smestad and Kautek [Smestad et al and Kautek; 1989].

Comparison between the photocurrents and the photovoltages of the samples A and B show a marked difference. These values increase by a factor of 8.0 (for photovoltage) and over 18.0 (for photocurrent) when the photoanode was annealed in vacuum and then etched in a solution of hydrogen fluoride, ethanoic acid and nitric acid mixed in the ratio of 1:1:2. It is argued here that the annealing (in vacuum) process may have helped improve the crystallinity of the iron pyrite film on the photoanode. This made electron movement through the film bulk easier and faster. Etching

helped in the removing of any surface or subsurface imperfections such as impurities on the film crystals and and mechanical damage on the iron pyrite surface, enhancing better electrical conduction. Ennaoui and others [Ennaoui et al, 1986] have also reported better results when iron pyrite was etched with the above solutions.

One possible cause of the observed low yield of photocurrents and photovoltages of the solar cell may be the loss of some photons due to surface reflection. The optical investigation of the cell container (Fig. 4.4) shows that its percentage transmittance between the wavelengths 400-700 nm ranges from 86.7 to a maximum of 92.0. For higher wavelengths, the transmittance remains almost constant at 92.0. Clearly, the cell-container was not 100% transparent to the radiation falling on it. Thus some photons could have been lost through reflection and absorption.

To minimize the absorption of the incident radiation by the electrolyte, the photoanode was placed as near the cell-container window as possible. However, it was not possible to make the space between the cell window and the photoanode totally electrolyte free. Thus there was still some radiation loss through absorption by the electrolyte. As noted from Fig. 4.3 the measured electrolyte optical transmittance varied from 0 at 480 nm wavelength to 52.9 at 600 nm. Thus within this region, there was quite a significant photon absorption.



Another possible reason for low values of photocurrents and photovoltages is the series resistance of the cell. The series resistances for the cell was  $8.0 \text{ k}\Omega$  with photoanode A and  $6.0 \text{ k}\Omega$  with photoanode B. A high resistance may be an indication of high power loss in the cell output. This high power loss is reflected in the amounts of photovoltage and photocurrent yielded by the cell. If the power loss is high due to high resistance, these values will be small. Low values of photovoltage, photocurrent and thus low efficiency due to high series resistance have been reported [Ennaoui and Tribusch, 1984].

We can also attribute the low photovoltage values to tentative impurity bands within the forbidden region which interfere with the band structure of the semi-conductor, thus affecting the photoanode performance. Iron pyrite has no lowspin configuration [Muller et al, 1990; Fiechter and Tribusch, 1990]. These unpaired spins caused by a deviation from the ideal composition introduces a band in the forbidden region thus diminishing the theoretically expected photovoltage. This is strongly supported by the fact that the chemicals used were only about 98% pure. This argument is also echoed by Muller [Muller, 1989].

The photoanodes used in our cell might have had micropinholes in the iron pyrite layer. When immersed in the electrolyte, these pinholes lead to a short circuit in the photogenerated current and effectively shunt the PEC solar cell. This shunting leads to low photocurrents and photovoltages.

Smestad [Smestad et al; 1989] has argued that if iron pyrite grains in the film are oriented such that many grain boundaries must be transversed by an electron from the bottom to the top before it finds its way to the external load, there will be a low photocurrent. Due to this long path of the electrons, some of them recombine with holes while others get trapped on the way. A significant loss of electrons is experienced which is reflected in the small amount of photovoltages and photogenerated currents. On the basis of our findings on photoanode B and photoanode A it can be argued that the non-vacuum-annealed sample may have had its grains oriented in such a way as to make it difficult for electrons to transverse from the bottom of the film to the top. Photoanode B had this problem reduced by the vacuum annealing process. Thus the it gave a higher value of photocurrent and photovoltage than A.

There is a very high possibility that the exposed junction in our cell could have affected our results negatively. The exposed junction might have enhanced the role of impurities and surface states. Boddy [Boddy, 1964] has reported significant effect even with an impurity concentration of as low as  $10^{-8}$  M. The interface between our semi-conductor and redox solution may have contained a number of chemical species including the products of the chemical or electrochemical reactions of the semi-conductor and the solution. All these have associated energy levels and thus contribute to the existence of surface states. In case the chemical impurities introduce a new state between the position of the conduction band in the semi-conductor bulk and its edge at the solution interface, the height of the barrier on which our solar cell is based may deteriorate. In the absence of the surface states, the photovoltage equals the difference between the dark and the illuminated positions of the band. If a surface state is present and if the total energy of the photovoltage and conduction band is

position of the conduction band in the semi-conductor bulk and its edge at the solution interface, the height of the barrier on which our solar cell is based may deteriorate. In the absence of the surface states, the photovoltage equals the difference between the dark and the illuminated positions of the band. If a surface state is present and if the total energy of the photovoltage and conduction band is greater than that of the surface state, electrons may tunnel to this state. This will effectively shunt the cell and a voltage loss at a certain photocurrent. The net effect is a reduction in the fill factor if the shunt is imperfect and in the open circuit voltage if the shunt is perfect.

#### 4.7 Spectral response of photoelectrochemical solar cell

Shown in Table 5.0 are the results of cell's spectral response. Fig. 4.7 is a graphical representation of Table 5.0.

Table 5.0 Spectral sensitivity of photoelectrochemical solar cell.

WAVE LENGTH $\lambda$ (MICRONS)	1.24	1.03	0.82	0.73	0.56	0.47	0.44	0.42
PHOTON ENERGEY (EV)	1.0	1.2	1.5	1.7	2.2	2.6	2.8	2.9
NORMALIZED PHOTOCURRENT (ARBITRARY UNITS)	0.12	0.59	0.92	1.00	0.82	0.78	0.76	0.67

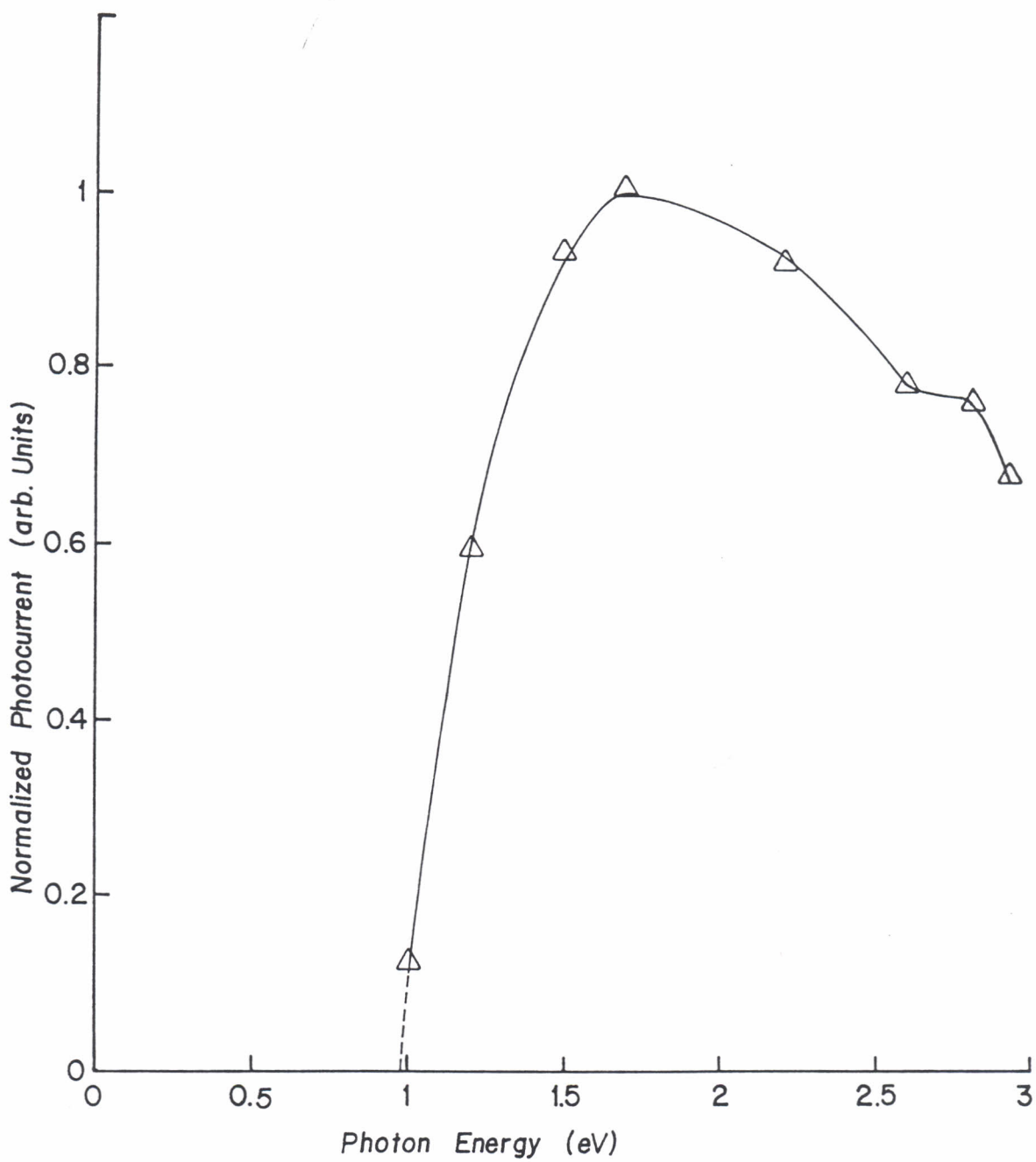


Fig. 4.7 Photoelectrochemical solar cell's response to wavelengths of varying energy

The spectral response of our cell was quite good as can be seen in Fig.4.7. The maximum value of the normalized photocurrent was obtained at a photon energy of 1.7 eV. The photocurrent then drops for higher and lower values of photon energy. Ennaoui and Tributsch [Ennaoui and Tributsch, 1984] have also obtained similar results.

#### 4.8 Stability of photoelectrochemical solar cell

The stability of the cell fabricated in our laboratory was observed over one period of a week with the results shown in Table 5.1.

Table 5.1 Values of photocurrent density obtained within a period of seven days for a PEC solar cell.

TIME (DAYS)	0	1	2	3	4	5	6	7
PHOTO CURRENT DENSITY ( $\mu\text{A}/\text{cm}^2$ )	8.0	7.0	6.2	5.6	5.2	5.1	5.1	5.1

The relationship between stability and time is depicted in Fig.4.8.

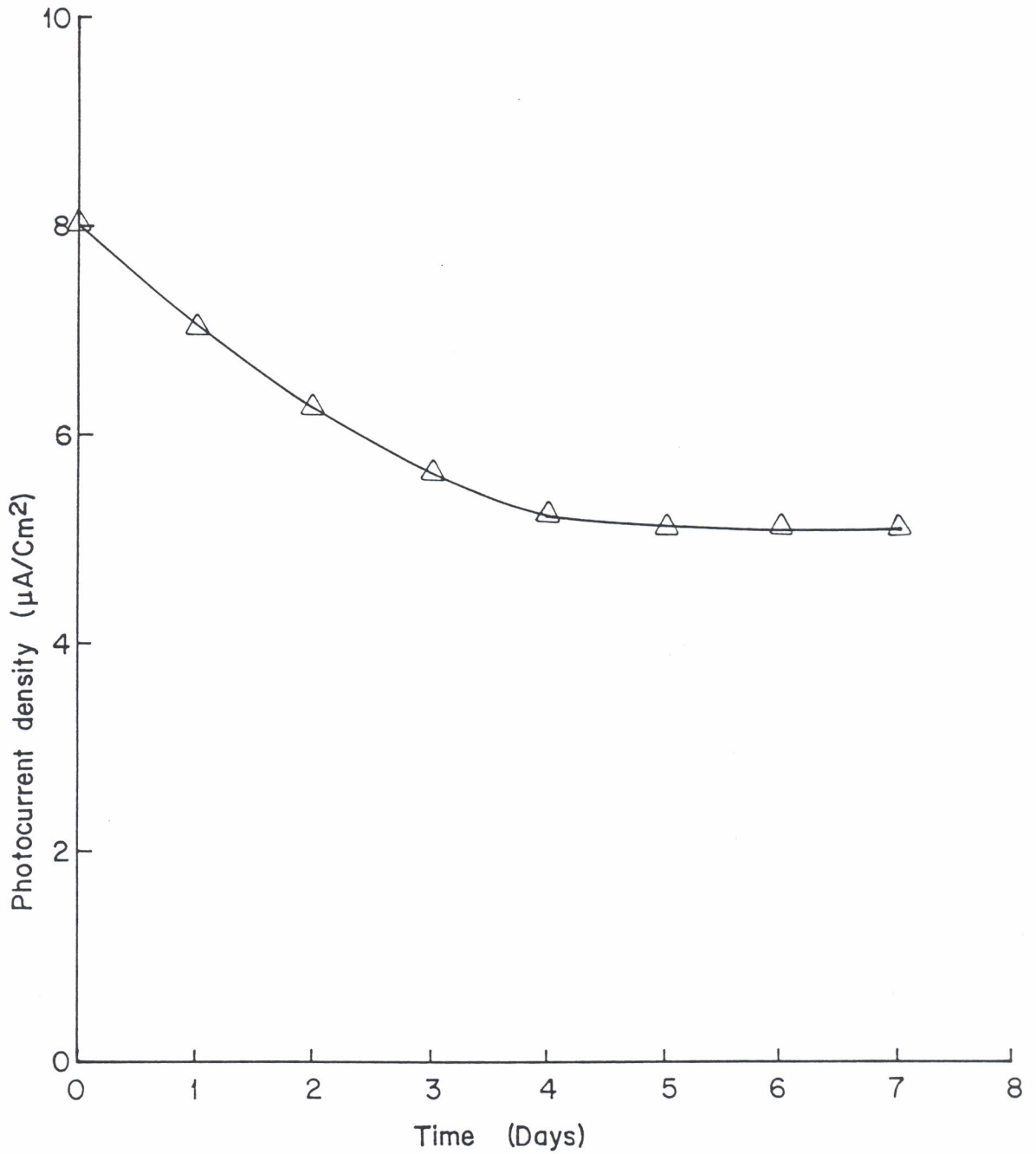


Fig. 4.8 Photocurrent density steadiness variation with time for photoelectrochemical solar cell .

The PEC solar cell was kept in a windowed carton and the whole setup kept in a dark room. The dark room was taken as of being of constant air mass.

It is observed that the solar cell's stability shows an initially high current density value at the early hours of operation dropping significantly within the first three days to assume a constant value thereafter. The relative stability can be attributed to the high concentration of I<sup>-</sup> ions in the electrolyte (3.0 M) [Ennaoui et al, 1993]. It has previously been demonstrated [Ennaoui et al, 1993] that the donating species can stabilize the photoelectrode against corrosion/photocorrosion if they are present in high concentration. This conclusion is also in agreement with other results [Ennaoui et al, 1986]; however, they used CaI<sub>2</sub>, HI and I<sub>2</sub> as redox solutions. Our findings seem to show some decay within the first three days and subsequent stability thereafter. The observed drop within the first three days can be attributed to the active role played by holes in eroding the photoanode. It is postulated here that there could be a tendency of the holes to attack the photoelectrode immediately after the cell starts operating before there is time for the electrons to reciprocate. However, after a time, there is stabilization as a space charge is created at the photoelectrode-electrolyte interface in which incoming holes get oxidized before they react with the photoelectrode.

## CHAPTER FIVE

### 5 CONCLUSION AND RECOMMENDATIONS FOR FUTURE WORK

#### 5.1 Conclusion

The present study aimed at the fabrication and subsequent characterization of an iron disulfide photoelectrochemical solar cell. Prior to the preparation of the iron disulfide as a photoanode by spray pyrolysis followed by sulfurization certain parameters had to be optimized.

The optimized deposition parameters in our study were spray rates of 14.0 ml/min, spray heights of 30-35 cm and substrate temperatures of 370.0 °C. The optimized annealing condition for iron pyrite were 4-5 °C/min on heating upto 350.0 °C and 1-2 °C/min on cooling down to 80.0° C; the entire time for annealing being 2.5-4.0 hrs. The absorption coefficient was determined as  $6.75 \times 10^4$  /cm at 800 nm.

Measured values of short circuit current density and open circuit photovoltage were  $40.0 \mu\text{A}/\text{cm}^2$  and 64.46 mv respectively. The cell gave a fill factor of 0.564 and an efficiency of  $2.71 \times 10^{-4}\%$ . Spray pyrolysis followed by sulfurization method has been successfully used in the growth of iron disulfide film for use as a solar material in our PEC solar cell. The values of photovoltage and photocurrent obtained are better than those obtained by some reseachers [Smestad and Kautek, 1989]. The spray pyrolysis method may in future claim dominance in thin film preparation if further improved.



## 5.2 Recommendations for future work

There are a lot of prospects for the development and advancement of PEC solar cells especially n-FeS<sub>2</sub>/I/I<sub>2</sub> solar cells. For further improvement, we recommend the following:

(i) The method of photoelectrode preparation needs to be improved. Even though every effort was made to make good adherent films, the spraying process needs improvement. There is need to make the spraying process automatic. Perhaps with the automation of the spraying process, new spray heights, rates and substrate temperatures may need to be investigated.

The spraying process should be carried out in a stable atmosphere i.e in an enclosed chamber where there is some good degree of atmospheric stability. This is to minimize dependence of the outcome on the environmental fluctuations.

An automated system should be fitted in place to maintain and monitor the substrate temperature. This would be more accurate in addition to making the reproduction of the work easier.

(ii) Future cell fabrications should be air free. This means evacuating all air out of the cell and sealing it. This might eliminate negative effects such as contamination of the electrolyte and the photoanode by dust particles and other impurities caused by exposure of the cell to the atmosphere.

UNIVERSITY OF NAIROBI  
HAROLD LIBRARY

(iii) The purity of all the chemicals used in the entire preparation right from the photoelectrode to the electrolyte should be of very high. Our chemicals were only about 98% pure.

(iv) The efficiency of our solar cell is quite low for any practical use. A detailed study of the chemistry of the deposited iron pyrite and the reactions at the semiconductor-electrolyte interface is needed to understand more what goes on and improve the cells' efficiency. Studies should also be carried out with the aim of understanding the effect, if any, of an exposed semi-conductor-electrolyte interface.

(v) Due to time factor, our cell was only tested for one week. More time should be devoted to the study of the cell's stability with the aim of making the cell more stable.

## REFERENCES

1. Abass A. K., Ahmed Z.A. and Tahir R.E. (1986), *Interband transitions of chemically deposited pyrite films in the fundamental absorption region between 1 and 3.8 ev*, *Phy. Stat. Sol., (A)* **97**, 243-247.
2. Abass A. K., Ahmed Z.A. and Tahir R.E. (1987), *Absorption edge measurements in chemically deposited pyrite FeS<sub>2</sub> thin layers*, *J. Appl. Phys.*, **61** (6), 2339-2341.
3. Angrivist S.W.,(1982), *Direct Energy Conversion*, 4<sup>TH</sup> ed., Allyn and Balon, Inc., Boston, 9.
4. Backus C.E., (1977), In: *Solar Energy Engineering*, Edit. by Sayigh, Academic Press, London, p. 263-285.
5. Beda p. and Kaiser D., Giles N.C, Lansari Y. and Schetzina J.F, (1987), *Electrical and optical properties of p- and as doped Cd<sub>1-x</sub> Mn<sub>x</sub> Te*, *J. of Appl. Phys.*, **62**, (4-6), 1352-1362.
6. Bockris J.O.M, (1959), *Modern Aspects of Electrochemistry*, Academic Press, New York, p 343-371.
7. Boer K.W and Piprek J. ,(1994), *Inverse delta doping for improvement of solar cells*, *J. of Appl. Phys.*, **75**, (10), 5095-5101.

8. Bolton J.R, (1977), *Solar Power and Fuels*, Academic Press Inc., London, p. 11-13, 77-106.
9. Birkholz M., Fiechter S., Hartmann A. and Tributsch H., (1991), *Sulfur deficiency in iron pyrite (FeS<sub>2</sub>) and its consequences for band structure models*, Physical Review B, **43**, No. 14, 11926-11936.
10. Bither T. A., Bouchard R.J., Cloud W.H., Donohue P.C. and Siemons W.J., (1968), *Transition metal pyrite dichalcogenides: High-synthesis and correlation of properties*, Inorg. Chem., **7**, 2208.
11. Cheremisinoff P.E and Regino T.C ,(1978), *Principles and Applications of Solar Energy*, Ann Arbor Science Publishers Inc., New York, p.141-156.
12. Ennaoui A. and Tributsch H., (1984), *Iron disulphide solar cells*, Solar Cells, **13**, 197-200.
13. Ennaoui A. and Tributsch H., (1985), *Light-induced electron transfer and photoelectrocatalysis of chlorine evolution at FeS<sub>2</sub> electrodes*, J. Electroanal. Chem., **204**, 185-195.
14. Ennaoui A., Fiechter S., Goslowsky H. and Tributsch H., (1985), *Studies of synthetic iron disulfide crystals grown by chemical vapour deposition (CVD)*, J. Electro Chem. Soc., **132**, 1579.
15. Ennaoui A., Fiechter S., Jaegermann W. and Tributsch H., (1986), *Band structure models for ideal stoichiometric FeS<sub>2</sub>*, J. Electro Chem. Soc., **133**, 97.

16. Ennaoui A., Fiechter S., Jaegermann W. and Tributsch H., (1986), *Photoelectrochemistry of highly quantum efficient single-crystalline n-FeS<sub>2</sub> (pyrite)*, J. Electro Chem. Soc., **133**, No.1., 97-106.
17. Ennaoui A., Fiechter S. and Tributsch H. and Giersig M., Vogel R. and Weller H.,(1992), *Photoelectrochemical energy conversion obtained with ultrathin organo-metallic-chemical-vapour-deposited layer of FeS<sub>2</sub> (pyrite) on TiO<sub>2</sub>*, J. Electrochem. Soc., **139**, No.9, 2514-2518.
18. Ennaoui A., Fiechter S., Petternkufer C.H., Alonso-Vante N., Buker K., Bronold M., Hopfner C.H. and Tributsch H., (1993), in: *Solar Energy Materials and Solar cells*, **29**, Elsevier Science Publishers, B.V., Netherlands, 289-370.
19. Ferrer I. J. and S'anchez C., (1991), *Characterization of FeS<sub>2</sub> thin films prepared by thermal sulfidation of flash evaporated iron*, J. Appl. Phys., **70**, (5), 2641-2647.
20. Ferrer I. J. De las Heras C. and S'anchez C., (1993), *Physical properties of Cu-doped FeS<sub>2</sub> pyrite thin films*, Applied Surface Science, **70/71**, 588-592.

21. Fiechter S., Mai J. and Ennaoui A. and Szacki W.,(1986), *Chemical vapour transport of pyrite ( $FeS_2$ ) with halogen (Cl, Br, I)*, J. of Crystal Growth, **78**, 483-444.
22. Flemming J.G., (1988), *Growth of  $FeS_2$  (pyrite) from Te melts*, J. of Crystal Growth, **92**, 287-293.
23. Fujishima M. and Honda K., (1972), *Electrochemical photolysis of water at a semi-conductor electrode*, Nature **238**, 37-38.
24. Fu-ren F.F., White H.S., Wheeler B.L. and Bard A. J., (1980), *Photoelectrochemistry and photovoltaic systems with n- and p-type  $WSe_2$  in aqueous solution*, J. Am. Chem. Soc., **102** (16), 5142.
25. Gerischer H. and Tobias C.W, (1978), *Advances in Electrochemistry and Electrochemical Engineering*, John Wiley and Sons, New York, p.1-30.
26. Ghanam M., (1994), *Photovoltaic, A College on Thin Film Technology*, **4**, Dar es Salaam, Tanzania.
27. Heller A. and Miller B.,(1976), *Semi-conductor-liquid junction solar cells based on anodic sulphide films*, Nature, **262**, 680-681.
28. Heller A. and Miller B.,(1980), *Some recent progress in semi-conductor-liquid junction solar cell*, Electrochimica Acta, **25**, 29-41.

29. Hopfner C., Ennaoui A., Ellmer K. and Fiechter S., (1993) in: *Multicomponent and Multilayered Thin Films for Advanced Microtechnologies: Techniques, Fundamentals and Devices* edited by Auciello O. and Engemann J., Kluwer Academic Publishers, Netherlands, P. 141-144.
30. Hopfner C., Ellmer K., Ennaoui A., Petten Kofer C., Fiechter S., and Tributsch H., (1995), *Stoichiometry-, phase- and orientation-controlled growth of polycrystalline pyrite (FeS<sub>2</sub>) thin films by MOCVD*, J. of Crystal Growth, **151**, 325-334.
31. Hovel H.J, (1975), *Semiconductors and Semimetal*, **11**, Academic Press, New York, p. 226-227.
32. Kastur Lal Chopra and Suhit Ranjan Das, (1983), *Thin Film Solar Cells*, Plenum Press, New York and London, 153-328.
33. Kivaisi R.T., (1994), *Determination of film thickness and deposition rate*, A College of Thin Film Technology, **1**, Dar es Salaam, Tanzania.
34. Lokhande C.D and Dhumre S.S, (1993), *Studies on photoelectrochemical storage cells formed with chemically deposited CdSe and Ag<sub>2</sub>S electrodes*, Solar energy materials and solar cells, **29** (2), 183-184.
35. Lona N., (1997), *Growth and properties of sprayed iron disulfide (FeS<sub>2</sub>) films*, Msc Thesis, University of Nairobi.

36. Lokhande C.D and Dhumre S.S, (1992), *Transcations of the SAEST*, **27**, No. 2-3, 141-145.
37. Lynn F.S. and Mark S.W., (1979), *Flat band potential of n- type semi-conducting Molybdenum disulfide by cyclic voltammetry of two-electron reductants: interface energetics and the sustained photooxidation of chloride*, J. Am. Chem. Soc., **101**(22), 6496.
38. Lynn F.S. and Mark S.W., (1980), *N-type Molybdenum diselenide-based photoelectrochemical cells: Evidence for Fermi level pinning and comparison of the efficiency for conversion of light to electricity with various solvent/halogen/halide combinations*, J. Am. Chem. Soc., **102** (23), 6964.
39. Memming R., (1980), *Solar energy conversion by photoelectrochemical processes*, *Electrochimica Acta* **25**, 77- 88.



40. Muller W., Bertschat H.H., Biechermann K., Kowallik R., Lahmer-Naim E., Mahnke H.E., Seeger S., and Zeltz W.D. and Fiechter S. and Tributsch H., (1990), *Perturbed-angular-distribution measurements of the chemical shift of iron in the disulfide FeS<sub>2</sub> (pyrite) and RuS<sub>2</sub> (laurite)*, Physical Review B, **41**, No. 13, 8624-8629.
41. Peter L.M., (1978), *The photoelectrochemical properties of anodic cadmium sulphide films*, Electrochimica Acta, **23**, 1073-1080.
42. Roy C.B, Nandi D.K, Mahapatra P.K., (1986), *Photoelectrochemical cells with n type ZnSe and n type Sb<sub>2</sub>Se<sub>3</sub> thin film semi-conductor*, Electrochimica Acta, **31** (10), 1227-1229.
43. Schieck R., Hartmann A., Fiechter S., Konen Kamp R. and Wetzch H., (1990), *Electrical properties of natural and synthetic pyrite (FeS<sub>2</sub>) crystals*, J. Mater. Res. **5**, No. 7, 1567-1572.
44. Shuey R.T., (1975), *Semiconducting Ore Minerals*, Elsevier, London, P. 304-318.
45. Smestad , (1990), *Photoactive thin films semi-conducting iron disulfide prepared by sulfuration of iron oxides*, Solar energy materials, **20** , 149-165.
46. Smestad G., Ennaoui A., Fiechter S., Tributsch H., Hofmann W.K., Birkholz M. and Kautek W., (1990), *Photoactive thin film semiconducting iron pyrite prepared by sulfurization of iron oxides*, Solar Energy Materials, **20**, 149-165.

47. Sihvonen in: Bolton J.R., (1977), *Solar Power and Fuels*, Academic Press Inc., London, p. 11-13, 77-106.
48. Solar Energy group-Physics Dept, University of Dar es Salaam, (1994), *Thin Film Technology*, Dar es Salaam, Tanzania.
49. Tokio O.,(1979), *Solar - Hydrogen Energy Systems*, Pergamon Press Limited, London, p. 137-154.
50. Weman H., Henry A., Begum T., Monema B., Awadelkarim O. and Lindshom J.L.;(1989), *Electrical and optical properties of gold-doped n-type silicon*, J. of Appl. Phys., **65** (1-3), 137- 144.
51. Williams J.R., (1977), *Solar Energy Technology and Applications*, Ann Arbor Science Publ. Inc., New York, p.18-20.